Archives of Civil and Mechanical Engineering (2023) 23:123
https://doi.org/10.1007/s43452-023-00665-z

ORIGINAL ARTICLE

# Development of hybrid performance-based optimization algorithm for structures equipped with vibration damper devices

**Al-jbury Najad Amer Ayyash**[1] · **Farzad Hejazi**[2]

Received: 7 September 2022 / Revised: 19 March 2023 / Accepted: 7 April 2023 / Published online: 20 April 2023


## Abstract

Nowadays, various types of vibration damping systems are being implemented in different buildings to diminish seismic effects on structures. However, engineers are faced with the challenging task of developing an optimum design for structures utilizing a proper type of damping device based on new techniques such as the performance-based design method. Therefore, this research was aimed at developing a multi-objective optimization algorithm by hybridizing the particle swarm optimization (PSO) and gravitational search algorithm (GSA) to obtain an optimum design for structures equipped with vibration damper devices based on the performance-based design method. Then, the developed hybrid algorithm (PSOGSA) would be capable of optimizing the damping system simultaneously with the optimized details of the structural sections, including the steel rebars, by satisfying all the design criteria. For this purpose, a special process for the design of structures equipped with vibration damper devices according to the performance-based design method was developed by considering of a wide range of vibration damping systems. The proposed PSOGSA optimization framework was then implemented to design a 12-storey reinforced concrete structure equipped with different types of dampers to minimize the structural weight while satisfying all the prescribed performance-based design acceptance criteria. The results indicated that the proposed optimization method was able to successfully optimize the details of the structural members as well as the type and properties of the damper, which significantly improved the structural response in terms of the formation of plastic hinges and the structural movements.

**Keywords** Hybrid optimization algorithm · Particle swarm optimization · Gravitational search algorithm · Seismic damper devices · Performance-based design

## 1 Introduction

The rapid growth of urbanization has resulted in a historic increase in the number of structures and high-rise buildings. Excessive vibrations in buildings are expected to be induced by external forces, such as earthquakes and winds. The induced vibrations may lead to structural damage and the unsatisfactory performance of structures. Induced vibrations can cause significant inconveniences, if not, casualties. Therefore, to enhance the safety and functionality of structures, control of vibrations in structural systems has long been considered by structural designers, and serves as a major source of technological competitiveness [1].

Many vibration control technologies, including damping, vibration isolation, control of excitation forces, and vibration absorbers, have been adopted to decrease the damage and amend the performance of structures. Each system has its own limitations and advantages, and the choice of a particular control system is usually decided by taking into consideration several factors, such as effectiveness, convenience, and life cycle cost [2].

The use of seismic control systems has increased, but choosing the best damper and installing it into a building are very important for reducing vibrations in structures when subjected to seismic loading. The controlling devices reduce damage significantly by increasing the safety and serviceability of the structure, and preventing the building from collapsing during an earthquake. Therefore, much research is being carried out to find the best solution [3].

✉ Farzad Hejazi
farzad.hejazi@uwe.ac.uk

[1] Department of Civil Engineering, University Putra Malaysia, Seri Kembangan, Malaysia

[2] Faculty of Environment and Technology, The University of The West England, Bristol, UK

Some technologies have been developed and adopted to control excessive vibrations, to mitigate their impact on the structural response, and to keep them within sustainable limits during unpredictable events, such as earthquakes [4]. To enhance their performance and ensure their functionality, civil infrastructures require reliable and efficient mechanisms to provide structures with the adequate capacity to maintain their structural integrity under such loadings. Therefore, seismic control systems are needed to enhance the structural behaviour, such as by increasing the energy-dissipation capacity of civil infrastructures [5].

Cha et al. [6] investigated multiple optimization methods to achieve several targets in which expense and reliability were concurrently optimized to obtain multiple hazard-stricken output levels. The direct performance-based design method developed by Cha et al. [7] provides multiple control design layouts for various efficiency levels with different risk levels, using multi-target optimization approaches. Based on the findings, the system stability method determines the storey with the highest total value of near drifts, enabling the seismic fragility of multi-storey buildings to be more precisely measured.

The Liapunov equation was used by García [8] to calculate the mean-square response of the random process and to improve the parameters of a pendulum tuned mass damper (PTMD). The results revealed that the performance of the optimized PTMD is improved when the structure has a linear hysteresis loop. The enhanced PTMD minimizes the mean value of the standard deviation of the principal structural displacement. Furthermore, for a variety of dynamic qualities, the optimized device using the suggested approach decreases vibrations, limits the development of plasticity, and protects the safety of the basic structure on soil. Xian et al. [9] provided an efficient optimization approach for large-scale non-linear viscous dampers that considered both the random seismic excitations and unpredictable damper parameters. To optimize the structure, the method of moving asymptotes (MMA) was applied. Under random seismic excitations, the suggested optimization framework was effectively applied to the stochastic optimum design of uncertain viscous dampers for a long-span suspension bridge. The results implied that, in addition to random seismic excitations, the uncertainty of damper settings must be addressed.

Moghaddam et al. [10, 11] proposed an optimum strength distribution method for the seismic design of tall buildings, and thereafter, Hajirasouliha et al. [12] implemented this method to develop a new performance-based optimization technique for RC frames with friction wall dampers [13] to reduce the computation cost [14].

The performance-based earthquake engineering (PBEE) philosophy is aimed at improving seismic risk decision-making using scientifically sound assessment and design procedures, which provide stakeholders with informed decision-making options. The first wave of PBEE procedures, such as FEMA-273 1997 [15], represented a significant advance towards standardized decisions. Relations would be formed between structural reaction indices (inter-storey drifts, inelastic deformations, and member forces) and performance-orientated definitions, such as immediate occupancy, life safety, and collapse prevention. The performance-based plastic design (PBPD) technique for the design of humpbacked braced frames (BRBFs) was proposed by Sahoo [16]. All the BRBFs tested in this analysis achieved the output goals for yield mechanisms and target drift speeds. As the PBPD is a straightforward design process, no iterations have been done to achieve the performance goals of the BRBF. Gaxiola-Camacho et al. [17] suggested a new reliability appraisal method for filling this expertise gap by providing an alternative to the existing design requirements for the protection of life. Giannakouras and Zeris [18] evaluated the direct displacement-based seismic design (DDBD) provisions for modelling such irregular RC structures and their seismic performance on non-linear static and dynamic analyses. The approach was viewed favourably by the engineering community through major changes that were suggested simultaneously. While the scope of its implementation is constantly expanding, for situations such as frames with a retrograde irregularity no specific guidelines are usually given, arguing that no fundamental changes to the method are expected in such situations. Guidelines are given to ensure that the DDBD approach is used to produce objective performance. Zhang and Tian [19] proposed an optimal seismic design framework for multi-storey reinforced concrete moment frames based on simplified results. The suggested solution minimizes building costs and integrates plastic rotation, and optionally, inter-storey drift as optimization constraints. The developed optimization method consists of two steps, deciding the feasible border region in the field of strength and rigidity, and maximizing the area of the material used.

Based on an extensive review of the literature, as discussed above, the main challenge was identified as the optimization of a structural design that is equipped with vibration damper devices according to the performance-based design method. Since the design of structures based on this method must satisfy a few acceptance criteria for the seismic response of structures, the approach employed is to select the best vibration dissipation type and properties simultaneously, while optimizing the structural members (beams and columns), which is a very complicated task using the conventional optimization techniques.

Therefore, this study attempted to mitigate the extreme effects of earthquake excitations on structures by improving the performance of supplemental vibration dissipation systems, and by optimizing the structural design. Since the optimization process, according to the performance-based

design method, must consider several effective parameters regarding the seismic response of structures in terms of structural nodal displacements, structural member forces, plastic hinges, and structural construction costs (building weights), a multi-objective optimization algorithm was developed to optimize all the related parameters at the same time. Since, in the literature the particle swarm optimization approach was unable to search whole parts of the problem (random selection) and resulted in a reduced optimization phase, therefore, in this study the particle swarm optimization (PSO) method was hybridized with the gravitational search algorithm (GSA) to optimize the performance of earthquake energy-dissipation systems simultaneously while optimizing the structural characteristics, including those of the beam and column sections and also the steel reinforcement details.

## 2 Development of special procedure for the implementation of the performance-based design method for structures equipped with damper devices

The performance-based design (PBD) method is being increasingly implemented in the design of various structures under seismic excitations. According to this method, the structural members are designed to satisfy predefined criteria for the seismic response of a structure corresponding to the performance of the structure under an expected hazard level. The general concepts of the performance-based design method and its procedures, such as the ASCE 7-10 [20] and ASCE 41-13 [21], can be implemented as seismic provisions in buildings.

The performance-based design method is focused on fulfilling the performance objective of a specific type of structure to suit seismic design code requirements through the sizing and detailing of structural members. However, over the last few years, numerous supplementary structural vibration control devices have been developed to reduce seismic damage in structures. These devices can be integrated into structures to improve their structural performance without modifying the size and properties of the structural members.

Therefore, this research attempted to implement the performance-based design (PBD) method on the design of a structure equipped with a vibration damper system. For this purpose, a seismic design process for structures with vibration damper devices according to the performance-based design method was proposed, as shown in Fig. 1, and demonstrated step by step as follows:

(1) Define the demand and performance level for the considered structure based on its importance factor and application.
(2) Select and scale a set of appropriate seismic acceleration records for both the Design-Basis Earthquake (DBE) and Maximum Considered Earthquake levels according to the considered site condition, as demonstrated in Sects. 11.4.3, 11.4.4 and 11.4.5 of the ASCE 7.
(3) Select and define the characteristics corresponding to the considered structural vibration damper devices to be implemented in the structure.
(4) Conduct a preliminary design of the structure according to the conventional codes such as the ACI 318–14 under the applied load.
(5) Develop a numerical model of the considered structure and the vibration control devices using the finite-element method to carry out dynamic non-linear time-history analyses under applied loads.
(6) Define and assign the details of the deformation-controlled components according to the performance-based design method to the structural members such as beams and columns.
(7) Determine multiple earthquake hazard levels based on spectral response acceleration parameters from seismic hazard maps for multiple performance levels. The targeted response spectrum is derived from spectral acceleration based on site class effects, and then, check if the building meets the predefined performance levels such as the inter-storey drift, maximum displacement, plastic hinges, and demand-to-capacity ratio of the members.
(8) Perform dynamic non-linear time-history analyses for the developed structure equipped with vibration damper devices under considered earthquake records at both the DBE and MCE levels.
(9) Review and check the results of the analysis for the response of the considered structure, including the inter-storey drift, plastic hinge formation in the structural members, maximum displacement of the structure, and the demand-to-capacity ratio (member force/section capacity) for structural members.
(10) If the acceptance criteria regarding the performance-based designed method are satisfied for the current structural design and the selected vibration damper devices, then the design process has been completed.
(11) If the structure fails to meet the acceptance criteria, then the design process is repeated from the third step by changing the damper properties or by considering another type of damper.
(12) If the structure still fails to meet the acceptance criteria after changing the damper properties or using another type of damper, then the design process is

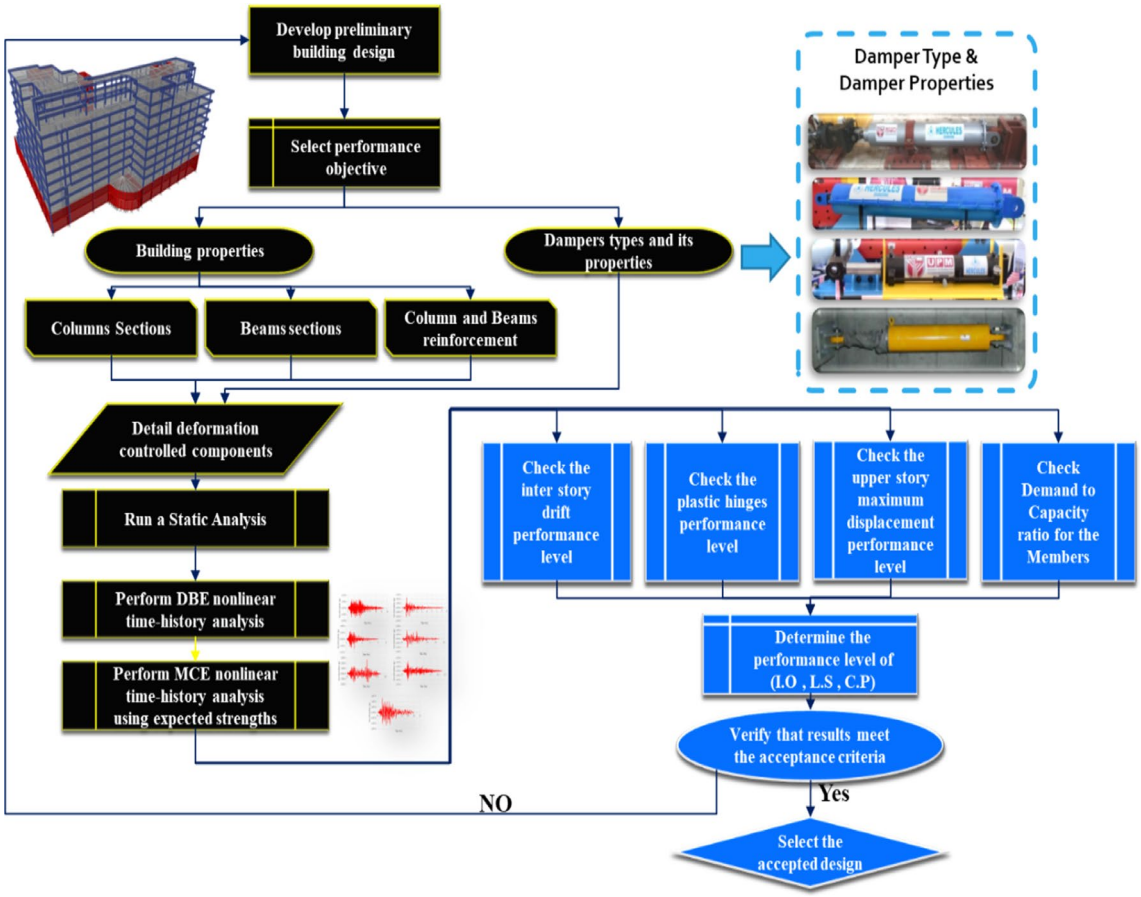


**Fig. 1** Performance-based design process for structures with a vibration damper system

repeated from the fourth step by resizing the structural member sections and proceeding to the next step.

More details for some of the above-mentioned steps are provided in the following sections.

## 2.1 Seismic acceleration record

Based on the site location and condition of the structure, a set of earthquake acceleration records were needed to select and scale to fit a continuum of 5% damped acceleration response consistent with Sect. 11.4.5 of the ASCE 7.

Probabilistic analyses of the seismic risk were performed for a degree of function (43-year return period duration as 50% over 30 years) to obtain the Overall Considered Earthquake Shakes, as defined in the ASCE 7 Parts 11.4.3 and 11.4.4, using the existing models to clarify regional seismic origins and earthquake prediction equations. According to Sect. 16.1.3 of the ASCE 7–10, a minimum of three accelerogram sets are required to evaluate the response background. Each chosen accelerogram collection must contain at least two horizontal components, and the vertical component can also be used in rare cases. The analysis needs adequate modes to contain at least 90% of the building weight for each main horizontal action direction.

The complete quadratic combination (CQC) formed blended model responses. The related response parameters, including forces and displacements, were used as the linear response parameters for the practical output calculation.

## 2.2 Preliminary design of the structure

The initial design of the structure in the specific seismic active region was made as the preliminary building design for concrete structures, according to the American codes ACI 318–14 [21]. The material nonlinearities for the structural components were implemented in the finite-element modelling of the considered RC structure, which reflected the inelastic behaviour of the building during strong earthquakes, as per the ASCE 41–13 [21]. The damping matrix was computed using Rayleigh damping, and the natural frequencies were determined to evaluate the time-domain reaction of the non-linear system. The Newmark time-step

integration method was used to evaluate the response of the structure under applied seismic records.

### 2.3 Checking the acceptance criteria

Each structural component was classified as primary or secondary prior to the determination of the conditions for the acceptance of the component. Then, the internal force in the structural elements and the deformation of the structure under an applied force were assessed in compliance with the specifications of the ASCE 41–13, Sect. 7.5.

The acceptance criteria for the concrete beams and columns were defined according to Table 10-7 and 10-8 in the ASCE 41–13. Also, the acceptance criteria for the steel beams and columns are presented in 9-6, ASCE 41–13.

It is commonly appropriate to use the mean demand for the response of a structure associated with the failure mode prediction to use a more restrictive behavioural mode demand, which may have catastrophic implications.

The storey drift ($\Delta$) design obtained from the analyses should not exceed 125% of the drift limit, as stated in the ASCE 7–10, Sect. 12.12.1. (2% of inter-storey drift). In addition, it is advisable to verify the formation of plastic hinges in the structural members in terms of the deformation ratios. Therefore, the degree and distribution of the inelastic specifications of current and new primary elements and components are specified by the demand-to-capacity ratio (DCR) for the considered structural components as:

$$\mathrm{DCR} = \frac{Q_{UD}}{Q_{CE}} \tag{1}$$

where $Q_{\mathrm{UD}}$ is the force due to gravity and earthquake forces measured in line with Sect. 7.5.2 of the ASCE 41-13; $Q_{\mathrm{CE}}$ is the predicted component strength or unit strength, as defined in the ASCE 41-13. The DCRs corresponding to the internal forces of the members such as the axial force, shears, and moments, shall be determined for each primary component of a structure. The essential operation of the component is the one with the highest DCR. The largest DCR in a considered storey is referred to as the essential aspect of the DCR in that storey. If there are several components in a specific storey, the element with the largest computed DCR, shall be identified as the essential component for that storey.

### 2.4 Failure to satisfy the acceptance criteria

If the response of the building under applied loads meets the acceptance criteria, then the accepted proposed damper type and characteristics, and details of the structural members (section size, diameter, and number for steel bars) are implemented in the design process; however, if it does not meet the acceptance criteria, then the structure is redesigned and its seismic response is checked again by selecting different characteristics for the damper device or using another type of vibration dissipation system. In this process, changing the properties of the damper is considered first, and the response is checked again against the criteria. However, if it does not pass the acceptance criteria, then consider changing the type of damper.

Furthermore, if the design is accepted regarding the damper properties and type, then consider redesigning for the member size to reduce the overall weight of the building, and thus, the cost of the structure. Once the redesigned structure passes the criteria, then the performance-based design process is completed.

## 3 Optimization of structure equipped with damper device using PSOGSA

An attempt was made in this research to develop an optimization procedure for the seismic design of a structure equipped with a vibration dissipation system according to the performance-based design method.

For this purpose, the multi-objective optimization method was considered to minimize many effective parameters on the response of a structure simultaneously during the optimization process.

Therefore, the PSOGSA computational method for optimizing a structure equipped with an anti-vibration system was developed by combining the particle swarm optimization (PSO) and gravitational search algorithm (GSA) to optimize the properties of the earthquake energy-dissipation system (damper devices) simultaneously, while optimizing the characteristics of the structure, including the size of the structural member sections, and the number and diameter of the steel rebars to satisfy the criteria for the performance-based design method by considering the structural displacement and force capacity of the structural elements such as the beam and columns.

### 3.1 Hybrid PSOGSA optimization method

The PSO method, which applies the concept of social interaction for problem-solving [22], is a robust stochastic optimization technique based on the movement and intelligence of swarms. It uses several agents (particles) that constitute a swarm moving around the search space looking for the best solution [23]. In this technique, each agent is considered as a particle, and in every given iteration, a particle will have a location and a velocity. The best position reached by the particles in an iteration is considered as the local best position, while the best position achieved across all iterations is considered as the global best position.

However, the PSO is not able to search in whole domains of the problem (random selection), resulting in an optimization process that is less accurate.

The gravitational search algorithm (GSA), which employs the gravitational law and laws of motion [24], has been applied successfully for solving various non-linear functions. The GSA has a flexible and well-balanced mechanism to enhance exploration and exploitation abilities.

Therefore, based on the advantages of the PSO method and the GSA algorithm, these methods were implemented in this study to develop a hybrid PSOGSA optimization technique to overcome the above-mentioned issues related to the individual PSO method and GSA algorithm.

### 3.2 PSOGSA optimization procedure

As mentioned before in this study, to optimize the type and properties of the structural damper device, and the details of the structural members for minimizing the effects of a seismic load on the structure, the multi-objective PSOGSA optimization method was adopted. Accordingly, the developed computational process for the proposed hybrid particle swarm optimization method and gravitational search algorithm (PSOGSA) was outlined in a flowchart, as illustrated in Fig. 2.

The computational process for the proposed hybrid PSOGSA multi-objective optimization method for the optimization of a structure equipped with damper devices was as follows:

1. The initial population of all the agents was generated as the first step which, in this study, represented the parameters for all the considered damper devices and the characteristics of the structure, including the section size for the beams and columns, and the number and diameter of the steel bars.
2. Each agent was considered as a candidate solution. Therefore, for each parameter, a random variable was assumed from the range within the upper and lower limits, which had already been set previously. For the beams and columns, predefined 20-section dimensions were considered. However, the diameter and number of steel reinforcements were defined within the specific range. For the characteristics of the damper devices, the upper and lower limits for the effective parameters on the damper performance were defined based on the available range of the considered devices in the market.
3. Then, during the optimization process, these values were selected randomly within the defined upper and lower limits, and based on the objective function in each iteration, the search pattern was changed within the predefined ranges to explore all the possibilities to find the optimum set.
4. Since, both the PSO and GSA methods were integrated as a single system to operate in parallel, although the particle updating for the PSO and GSA was identical, however, the velocity at which the changes were updated was different for both algorithms.

The PSOGSA method substituted the local search of the original PSO with the acceleration of the GSA, which was basically a local best and worst attentive search function. As a result, the suggested algorithm was

$$\begin{aligned} \mathrm{Vi}\,(\mathrm{t}+1) &= \mathrm{w} \times \mathrm{Vi(t)} + \mathrm{c1} \times \mathrm{rand} \times \mathrm{aci(t)} \\ &\quad + \mathrm{c2} \times \mathrm{rand} \times (\mathrm{gbest} - \mathrm{Xi(t)}), \end{aligned} \tag{2}$$

where Vi(t + 1) is the velocity of agent *i* at iteration *t* + 1, w is a weighting function, Vi(t) is the velocity of agent *i* at iteration *t*; cj is an acceleration coefficient, rand is a random number between 0 and 1, aci(*t*) is the acceleration of agent *i* at iteration *t*, gbest is the best solution so far, and Xi(t) is the position of agent i at iteration t.

i) Finally, the positions of the agents were updated by

$$\mathrm{Xi}\,(\mathrm{t}+1) = \mathrm{Xi}\,(\mathrm{t}) + \mathrm{Vi}\,(\mathrm{t}+1) \tag{3}$$

ii) The process of updating the velocities and positions would be stopped when an end criterion was met.

### 3.3 Optimization variables

The optimization variables in this study were split into two types in relation to the damper properties and structural characteristics, as demonstrated below:

**A-** Type and characteristics of the structural anti-vibration systems:

A-1- Damper Type (A).
A-1–1- First parameter for Damper Type (A).
A-1–2- Second parameter for Damper Type (A).
A-1–3- Third parameter for Damper Type (A).
A-2- Damper Type (B).
A-2–1- First parameter for Damper Type (B).
A-2–2- Second parameter for Damper Type (B).
A-2–3- Third parameter for Damper Type (B).
A-3- Damper Type (C).
A-3–1- First parameter for Damper Type (C).
A-3–2- Second parameter for Damper Type (C).
A-3–3- Third parameter for Damper Type (C).
A-4- Damper Type (…).

**B-**The details of the structural members, including the section size and details of the steel bars (number and diameter of steel rebars):

B-1- Beams:
B-1–1- Dimension for Beam Section.

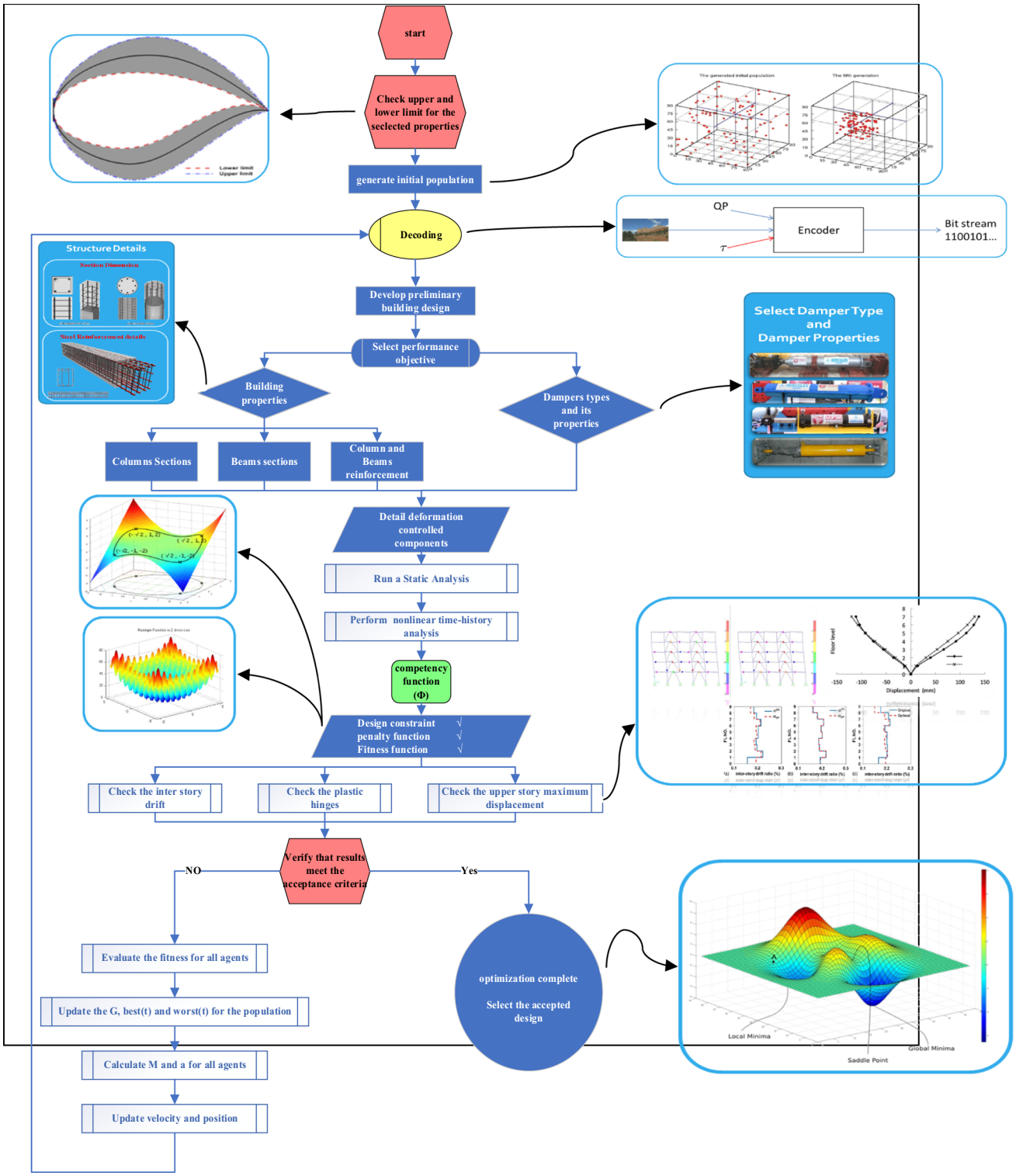


**Fig. 2** Development of computation algorithm for hybrid PSOGSA method to optimize a structure equipped with vibration damper devices according to the performance-based design method

B-1–2- Details of Steel Bars in the Beam Section.

B-1–2-1: Number of Steel bars in the considered Beam Section.

B-1–2-2: Diameter of Steel bars in the considered Beam Section.

B-2- Columns:

B-2- Beams:

B-2–1- Dimension for Column Section.

B-2–2- Details of Steel Bars in the Column Section:

B-2–2-1: Number of Steel bars in the considered Column Section.

B-2–2-2: Diameter of Steel bars in the considered Column Section.

As demonstrated, the first variables included the type of damper device and the characteristics of each structural anti-vibration system (damper devices), where these specific parameters influenced the function of the considered damper device.

Also, the second variables were related to the structural section details, including the section size of beams and columns, and the number and diameter of the steel rebars in each section.

In each iteration, the damper type was changed. It was a randomly selected agent from all the available choices of dampers, and was mixed with the best results (best agents) obtained through the fitness function from previous generations to have the benefit of the best yet results (from previous generations), and to have a chance of searching and assessing better agents from other available options (other damper devices). Although there may be a few redundant optimization generations, it will avoid any risk of missing any possibility of searching for better agents (better results). However, by considering the capability of the PSOGSA for fast convergency, and using advanced computation technologies and facilities, a few redundant generations were not effective in the overall optimization computation time in comparison to other available techniques.

### 3.4 Objective function of optimization

The hybrid PSOGSA optimization method is an advanced technique that focuses on the high ability of the hybrid optimization algorithm to optimize multi-objective problems. Most of the studies available in the literature regarding structural optimization considered either the weight of the structure as representing the considerable cost of construction as an objective function or only the displacement response of the structure as a structural stability optimization target.

However, this research was aimed at minimizing the weight of the structure by reducing the section area of the beams, columns, and steel bars, while considering the acceptance criteria regarding the performance-based design method, which included the structural movement and the structural member forces. Therefore, all these parameters were defined as the objective function for the developed hybrid optimization method.

An inelastic time-history analysis was conducted by implementing at least seven time-history seismic record data according to the ASCE 7-10 to determine the seismic response of the structure.

Then, the peak storey drift (positive and negative for the right and left side movements, respectively) was used to determine the critical state of the structural deformation using the objective function.

Since the structure experienced different storey drifts in various directions, therefore, the maximum movement of the structure in 3 perpendicular directions of $X$, $Y$ (horizontal movement) and $Z$ (up-down movement) for each earthquake was considered in the optimization process. However, since the vertical seismic response of the building was less than the horizontal movement, thus, the vertical displacement had no significant effect on the optimization process.

The following equations were formulated to determine the effects of displacements in all directions, and the structural weight during the optimization process:

$$D_x = \sum_{i=1}^{n} \frac{\Delta x_{i+1} - \Delta x_i}{h_i} \tag{4}$$

$$D_y = \sum_{i=1}^{n} \frac{\Delta y_{i+1} - \Delta y_i}{h_i} \tag{5}$$

$$W_t = \sum W_C + \sum W_B + \sum W_s \tag{6}$$

where $D_x$, $D_Y$ are the sum of the peak inter-storey drifts in the $X$- and $Y$-directions, $\Delta_x$ and $\Delta_y$ are the relative displacements in storey $i$ in the $X$ and $Y$-directions, respectively, $h_i$ is the height of storey $I$, and $n$ is number of storeys. Also, $W_t$ is the overall structural weight, $\Sigma W_C$ is the total weight of the columns, $\Sigma W_B$ is the total weight of the beams, and $\Sigma W_s$ is the total weight of the steel reinforcement.

Since the displacements in each direction were in different ranges and independently affected the optimization process, therefore, to scale the displacements in the same range, the moderation coefficients, $\emptyset_x$ and $\emptyset_y$, were multiplied with the sum of the inter-storey drifts in the corresponding $X$ and $Y$-directions. Similarly, a moderation coefficient of $\emptyset_t$ was multiplied with the sum of the weight of the beams, columns, and steel rebars to scale both the displacements and weights to have an equal impact on the objective function. Thus, the objective function was proposed as follows:

$$fobj = (D_X \times \emptyset_X) + (D_Y \times \emptyset_Y) + (Wt \times \emptyset_W) \tag{7}$$

### 3.5 Optimization design constraints

The optimization design constraints adopted in this research included the number of plastic hinges in all the structural members for the loading and unloading events during earthquake excitation. Thus, to consider the optimization design constraints, the penalty function was defined as follows to add it to the objective function:

$$p = \sum_{i=1}^{nc} CPHi \times PHi \tag{8}$$

where $P$ is the penalty function, and $PHi$ represents the design constraint, which is the total number of plastic hinges in the structural members. In this equation, $CPHi$ denotes the adjusted coefficient for constraints. A large value was prescribed for $CPHi$ to avoid the occurrence of plastic hinges. Therefore, during the optimization process, the PSOGSA was aimed at circumventing any occurrence of plastic hinges in the structural members (as the optimization constraint) while minimizing structural movements in all three directions in all the storeys (as the objective of the optimization). This was possible through the execution of the penalty function. Then, an auxiliary function was obtained by adding the penalty function to the objective function in the following form:

$$\Phi = fobj + p \tag{9}$$

where $\Phi$ is the competency function or the equivalent free function.

## 4 Considered damper devices

Numerous types of structural vibration damping devices have been developed over the past few years to dissipate vibrations and minimize harmful seismic effects on structures. This equipment is installed in structures as supplementary damping systems to enhance the structural efficiency and stability, without changing the size and properties of the structural members.

In this study, various types of structural damping devices were implemented to enhance the seismic performance of the structure through the dissipation of applied vibrations to the structure. The damper devices that were considered in this study were: oil damper [25], Bingham damper [26], fluid damper, friction damper [27], viscous wall damper [28], viscoelastic (rubber) bracing damper (RBD), rubber wall damper, yielding brace framework (YBF), and volumetric rubber bracing.

The details and optimization parameters for the damper devices that were considered in this study are outlined in the following sections:

### 4.1 Oil damper

An oil damper works by generating a drop in pressure when a viscous fluid passes through a valve or orifice in the piston within the cylinder during movement of the piston, as shown in Fig. 3. The generated damping resistance force in the oil damper is dependent on the speed of the movement and is not greatly affected by the temperature.

The parameters that were considered for a minimum damping force of 250 kN were 110 KN/mm for the internal rigidity (stiffness) and 2000 kN for the maximum damping force with an internal rigidity of 430 KN/mm.

The damping force of the oil damper is a function of the velocity of movement, as shown in the following equation:

$$\mathrm{F} = \mathrm{C_m} * \mathrm{V_d} \tag{10}$$

where $C_\mathrm{m}$ is the non-linear viscosity coefficient and $V_\mathrm{d}$ is the speed of movement.

The upper and lower limits that were considered for the effective parameters of the oil damper are listed in Table 1.

### 4.2 Bingham damper

A Bingham damper is made of a silicon-based filling material, steel cylinder, piston, and rod, as shown in Fig. 4. The minimum damping resistance force that was considered was 150 kN, with a non-linear viscosity coefficient of 88.3 KN/(s/mm)$^{0.1}$, while the maximum damping force that was considered was 2000 kN, with a non-linear viscosity coefficient of 1177.4 KN/(s/mm)$^{0.1}$.

The damping resistance force ($F_\mathrm{d}$) is expressed as

$$F_d = C_d \times \mu_d^{0.1} \tag{11}$$

where, $C_\mathrm{d}$ is the non-linear viscosity coefficient and $\mu$ is the speed.

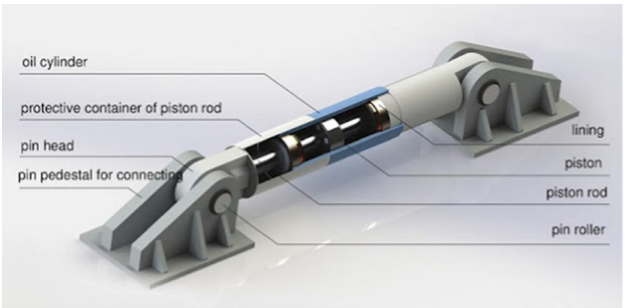


**Fig. 3** Oil damper components

**Table 1** Upper and lower limits for effective parameters for all the dampers considered in this study

| Device | Parameters | | | | | | |
|---|---|---|---|---|---|---|---|
| Oil damper | Type | Damping coefficient ($C_d$) | | | Stiffness ($K_e$) | | |
| | OD 1 | 493.2 kN×s/m | | | 110 kN/mm | | |
| | OD 2 | 585.8 kN×s/m | | | 430 kN/mm | | |
| Bingham damper | Type | Viscosity coefficient KN/(s/mm)$^{0.1}$ | | | Damping force (kN) | | |
| | BD 1 | 88.3 | | | 150 | | |
| | BD 2 | 1,177.4 | | | 2,000 | | |
| Friction damper | Type | Slip load (KN) | Stroke (mm) | Mid-stroke length (mm) | | Thickness (mm) | Damper mass (kg) |
| | FD 1 | 1,500 | ±175 | 2,200 | | 185 | 395 |
| | FD 2 | 450 | ±50 | 780 | | 175 | 115 |
| Viscous wall damper | Type | Stiffness (KN/mm) | | Damping (KN×s/mm) | | | Damping exponential coefficient |
| | VWD 1 | 78.8 | | 18.91 | | | 0.5 |
| | VWD 2 | 74.4 | | 21.89 | | | 0.5 |
| | VWD 3 | 71.8 | | 26.26 | | | 0.5 |
| RBD damper | Type | Stiffness (KN/mm) | | | Damping (KN×s/m) | | |
| | RBD 1 | 30.315 | | | 108.35 | | |
| | RBD 2 | 90.946 | | | 108.35 | | |
| Rubber wall damper | Type | Effective stiffness (KN/m) | | | Effective damping (KN×s/m) | | |
| | RWD 1 | 5,523 | | | 186.09 | | |
| | RWD 2 | 4,397 | | | 63.76 | | |
| Volumetric rubber bracings | Type | Stiffness (kN/m) | | | Damping (kN×s/m) | | |
| | VCR 1 | 9,118.3 | | | 114.3 | | |
| | VCR 2 | 12,413.1 | | | 158.6 | | |

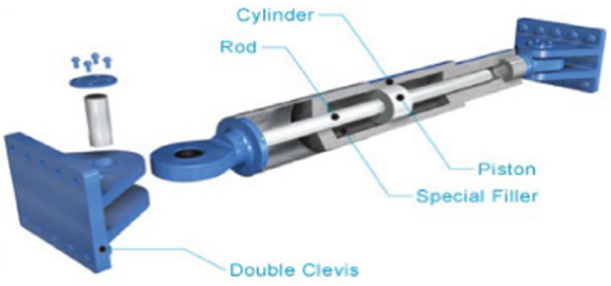


**Fig. 4** Bingham damper components

### 4.3 Friction damper

A friction damper is made up of a series of steel plates that have been specially treated to increase friction. These plates are clipped together and allowed to slip when subjected to a pre-set load, as illustrated in Fig. 5.

Friction dampers are designed to prevent slipping under small vibrations such as wind conditions, and they function only when subjected to high vibrations such as a seismic event. The lower limit is generally about 130% and the upper limit is about 75% of the shear force, after which the components of the friction damper will start to fail. In this study, two friction dampers were implemented, and the parameters that were considered for both these friction dampers are listed in Table 1.

### 4.4 Viscous wall damper

A viscous wall damper (VWD) consists of a stiffened steel tank filled with high-viscosity fluid and one or more steel vanes that extend into the tank of viscous fluid. The VWD is installed between two rigid girders within the floors, and the tank is connected to the floor, while the vanes are connected at the above level to dissipate the inter-storey movement, as illustrated in Fig. 6. Table 1 presents all the parameters that were considered for the viscous wall damper in this study.

### 4.5 Rubber bracing damper (RBD)

The developed viscoelastic (rubber) bracing damper (patent No: US20190323183 A1) consists of a steel tube cylinder with a steel inner core moving inside the cylinder. A high damping viscoelastic material, such as high damping rubber, is mounted between the inner core and outer tube, and is bound to both surfaces as energy dissipater members to absorb vibration loads, as shown in Fig. 7.

The resistance force of the device is a function of the effective stiffness and effective damping of the device,

**Fig. 5** Friction damper

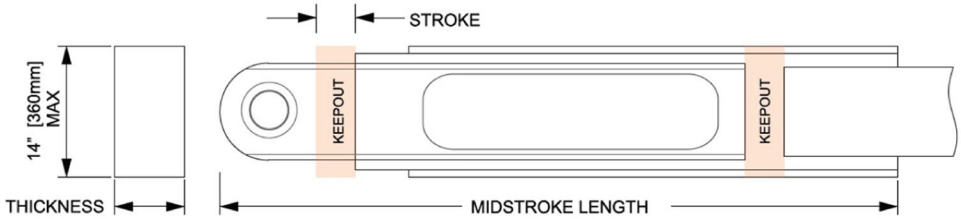


(a) Schematic representation

(b) Photos of a damper

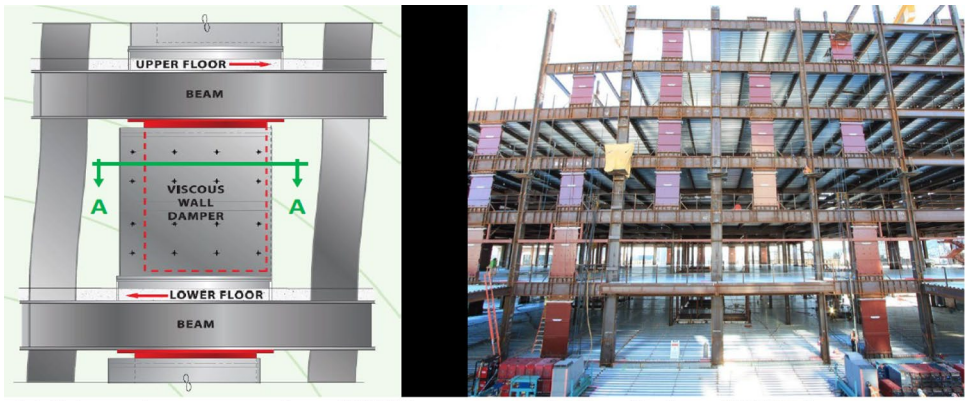


(a) Schematic representation of VWD **(b)** Installation of VWD in structure

**Fig. 6** Viscous wall damper. (**a**) Schematic representation of VWD, (**b**) Installation of VWD in structure

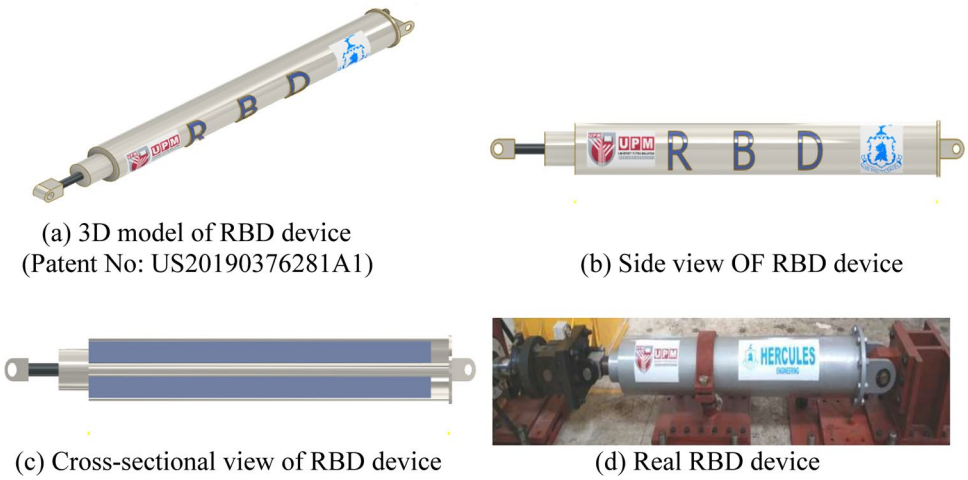


(a) 3D model of RBD device (Patent No: US20190376281A1)

(b) Side view OF RBD device

(c) Cross-sectional view of RBD device

(d) Real RBD device

**Fig. 7** RBD damping devices

where both these parameters are obtained from the hysteresis response of the RBD damper device via an experimental test. The upper and lower ranges that were considered for these parameters for the RBD damper are presented in Table 1.

### 4.6 Rubber wall damper (RWD)

As shown in Fig. 8, a rubber wall damper (Patent No: US10669734B2) consists of a few parallel steel panels that are bound to each other by high damping rubber. It is positioned within floors as wall panels. These dampers are highly capable of dissipating vibration energy and reducing the effects of earthquakes on structures to protect them against severe seismic excitations.

The damping force of a rubber wall damper is calculated using the following equation:

$$F_{VWD} = C_{VWD} \times V^{\eta} \tag{12}$$

where $F_{VWD}$ is the damping force, $C_{VWD}$ is the damping coefficient of the rubber wall damper, $V$ stands for the inter-storey velocity, and $\eta$ is the exponential coefficient for the velocity, which is in the range of 0.5–2.0. In this study, two types of rubber wall dampers were considered, where their corresponding parameters in terms of effective stiffness and effective damping are listed in Table 1.

### 4.7 Volumetric compression *restrainer (VCR)*

The developed volumetric compression restrainer device (patent No: US10914093B2) consists of a steel tube cylinder with a steel inner core moving inside the cylinder. Several steel divider plates are welded perpendicularly to the inner core and outer cylinder in parallel with each other, and the circular tubes made by the hyperplastic rubber are positioned in the spaces between the divider plates as energy dissipater members, as shown in Fig. 9. During movements of the shaft due to the vibration of a structure, rubber cubes are compressed between the divider plates and act in volumetric compression to generate a noticeable resistant force against the movement and to restrain the vibration. Two types of VCR devices were considered

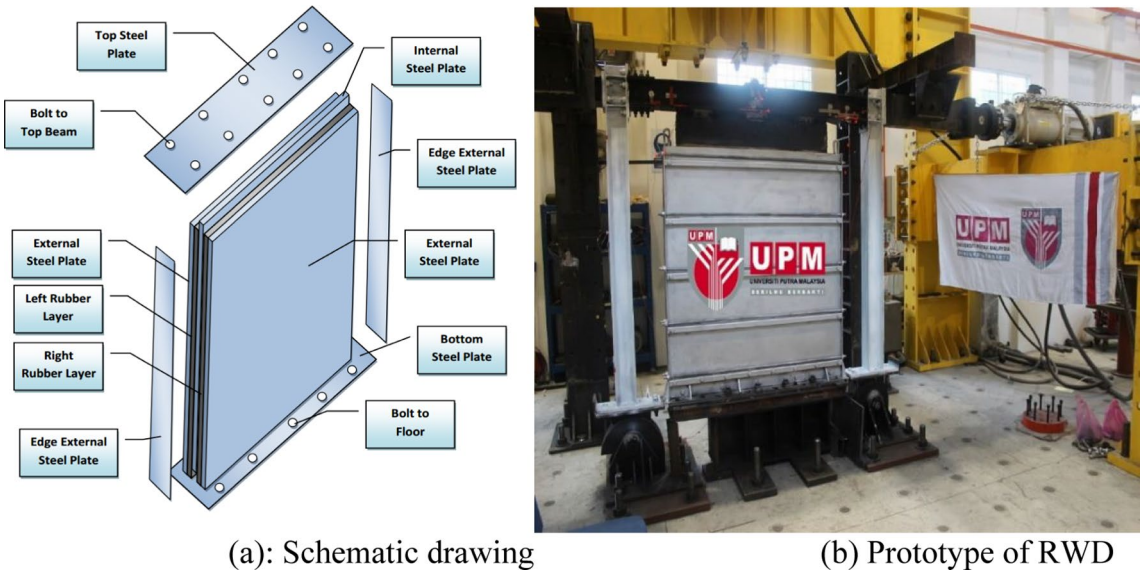


**Fig. 8** Details and components of rubber wall damper

**Fig. 9** Volumetric rubber bracing device

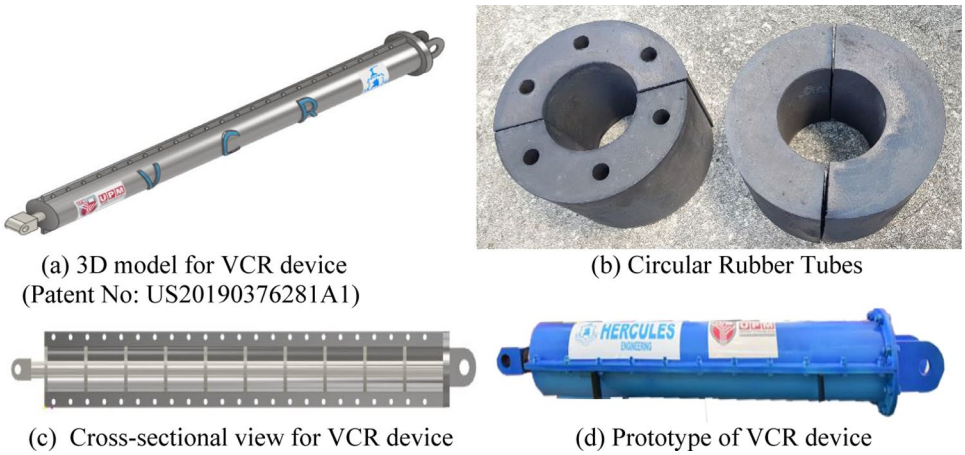


in this study, and the effective stiffness and damping corresponding to each VCR device is presented in Table 1.

### 4.8 Comparison between considered damper devices

A comparison was made of the different damper devices that were considered in terms of their range of performance (damping, stiffness, and stroke), installation condition, and components and details, as listed in Table 2.

As can be seen, among all the damper systems that were considered, the rubber wall damper and volumetric damper devices were the strongest dampers to generate a resistant force against the applied excitation force.

## 5 Integrated synchronized computation system

In this study, the ETABS finite-element program was implemented to conduct a structural seismic analysis, and, the PSOGSA optimization algorithm was codified in the MATLAB program platform. Therefore, the MATLAB and the ETABS programs were integrated and synchronized, whereby the data on the structural details were sent to ETABS, and a non-linear analysis of the structure under an applied seismic load was then performed, after which, the retrieved structural seismic response data were sent to MATLAB for the optimization process to be continued. Then, the data were resent again to the ETABS software.

**Table 2** Comparison of different damper systems considered in this study

| Damper type | Range of damper performance (Range is dependent on the available size of the device in the market) | | Installation Condition | Components |
|---|---|---|---|---|
| Oil damper | Damping coefficient (kN × /m) | 493.2 ~ 585.8 | Installed as a diagonal bracing within 2 node joints | Oil cylinder, protective container of piston rod, lining, piston, piston rod |
| | Stiffness (kN/mm) | 110 ~ 430 | | |
| Bingham damper | Viscosity coefficient KN/(s/mm)$^{0.1}$ | 88.3 ~ 150 | Installed as a diagonal bracing within 2 node joints | Cylinder, rod, silicon-based filling material, piston |
| | Damping force (kN) | 1,177 ~ 2,000 | | |
| Friction damper | Slip Load (KN) | 450 ~ 1,500 | Installed as a diagonal bracing within 2 node joints | Series of steel plates that have been specially treated to increase friction. These plates are clipped together and allowed to slip when subjected to a present load |
| | Stroke (mm) | ± 50 ~ ± 175 | | |
| | Mid-stroke length (mm) | 780 ~ 2,200 | | |
| | Thickness (mm) | 175 ~ 185 | | |
| | Approximate Damper Mass (kg) | 115 ~ 395 | | |
| Viscous wall damper | Stiffness (KN/mm) | 71.8 ~ 78.8 | Installed as a wall panel system within 4 node joints | Stiffened steel tank, high-viscosity fluid, steel vanes that extend into the tank of viscous fluid |
| | Damping (KN × s/mm) | 18.91 ~ 26.26 | | |
| | Damping Exponential Coefficient | 0.5 | | |
| Rubber bracing damper | Stiffness (KN/mm) | 30.315 ~ 90.946 | Installed as a diagonal bracing within 2 node joints | Steel tube cylinder, steel inner core moving inside the cylinder, high damping rubber is mounted between the inner core and outer tube |
| | Damping (KN × s/m) | 108.35 | | |
| Rubber wall damper | Effective Stiffness (KN/m) | 4,397- 5,523 | Installed as a wall panel system within 4 node joints | Parallel steel panels, high damping rubber, bolted to beams and floors |
| | Effective Damping (KN × s/m) | 63.76 ~ 186.09 | | |
| Volumetric rubber bracing | Stiffness (kN/m) | 9,118 ~ 12,413 | Installed as a diagonal bracing within 2 node joints | Steel tube cylinder, steel inner core moving, number of steel divider plates, hyperplastic rubber |
| | Damping (kN × s/m) | 114.3 ~ 158.6 | | |

This loop was repeated through the whole optimization process, perhaps up to hundreds and thousands of times, until the optimization convergency criteria were satisfied, thereby successfully ending the optimization process.

The two programs were synchronized through the creation of an executable file for the ETABS program, which was implemented using the MATLAB program during the optimization process to receive the structural data (details about the geometry of the structure, structural members, material, boundary conditions, loads, dampers, and isolator devices) from MATLAB, after which the time-history seismic analysis was run. Next, the ETABS executive program sent back the related data regarding the seismic response of the structure in terms of the nodal displacements, structural member force, and the plastic hinges that appeared in the structural members for different applied earthquake loads at different levels of performance for the structure. Then, after sending all the analysis results to MATLAB, the ETABS executive program was closed to be called again using the MATLAB program in the next iteration of optimization.

The executable file for the ETABS program was created using Visual Studio and by choosing Visual Basic as the coding language. Furthermore, the link between the executable file and ETABS was done through the API documentation provided by ETABS (CSI), as shown in Fig. 10.

## 6 Application of developed PSOGSA method for optimization of 12-storey RC structure

The developed PSOGSA method was implemented to optimize the seismic design of a 12-storey structure under considered earthquakes according to the performance-based design method.

As shown in Fig. 11, the considered structure in this research was a 12-storey, 3-by-5 bay reinforced concrete

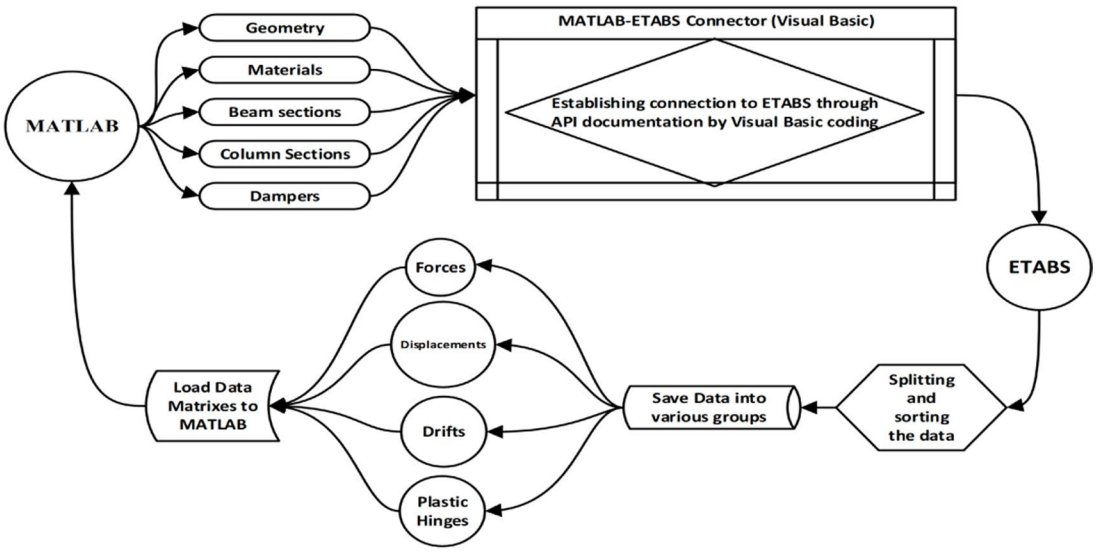


(a): Schematic view of the integrated synchronized computation system

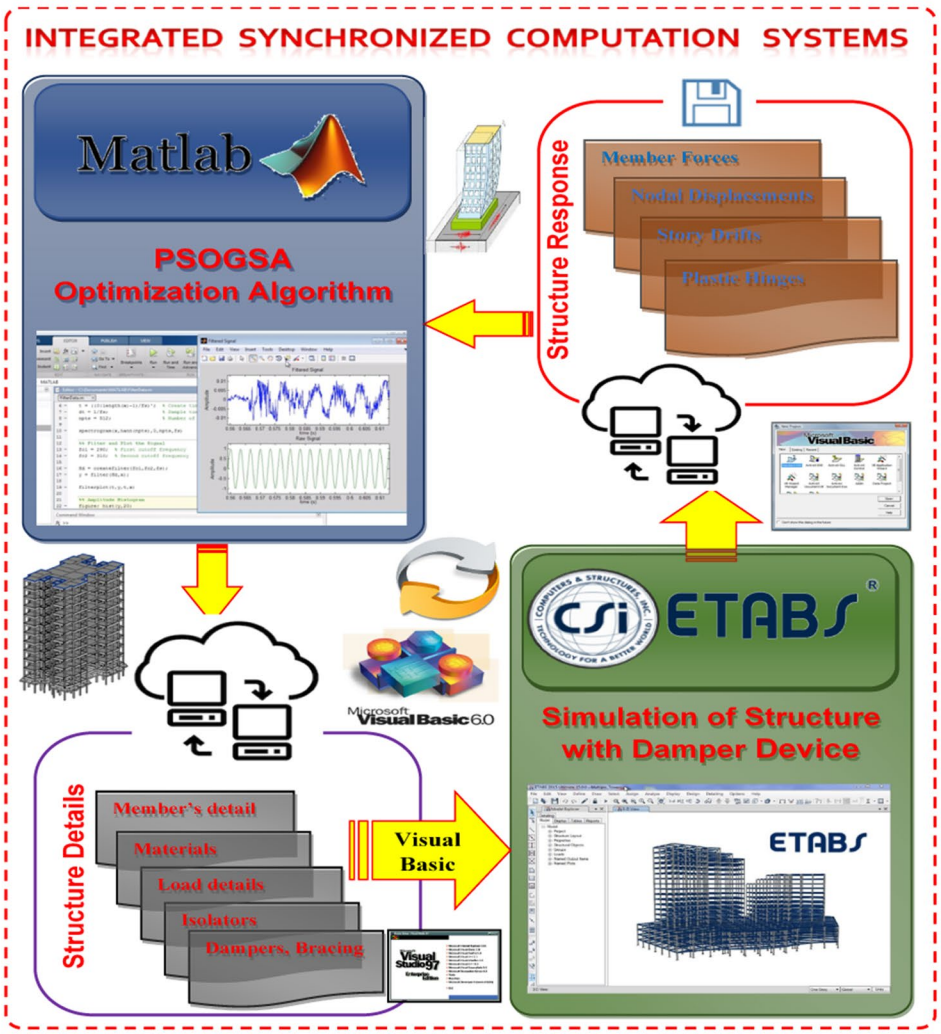


(b): Details of the Integrated Synchronized Computation Systems

**Fig. 10** Integrated synchronized computation systems

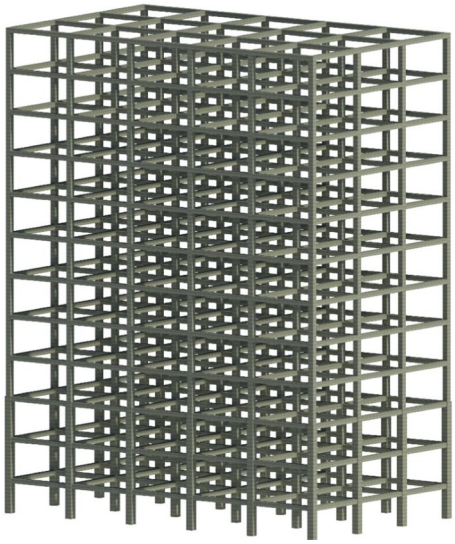

**Fig. 11** Geometry and FEM model of the considered 12-storey RC structure

moment resistant frame structure, which was designed and studied by Rahman at el. [29] based on the ASCE 7-10 code of provision. The height of the first floor was 4.27 m, and the height of the other floors was 3.66 m each, resulting in a building with a total height of 44.5 m. The width and length of the structure was 21.96 m and 36.6 m, respectively.

The columns were positioned 7.32 m apart from each other in both directions. The building was used as a commercial building/office. The seismic importance factor (I) was considered as 1.0. The building was in San Francisco, USA and situated in a high-seismic region. The acceleration spectral response parameters were determined as SS = 1.83, s1 = 0.85, position class D and stiff soil.

The system was categorized into risk Category II, with a seismic category E as per the ASCE 7–10, based on the short reaction acceleration parameters (SDS = 1.22 g at 0.139 s) and long period (SD1 = 0.85 g at 1 s). The columns and beam members were designed and detailed according to the ACI 318–14, using a compressive strength of f′c = 48 MPa for the concrete, and a yield strength of fy = 414 MPa for the steel reinforcement (ASTM Gr. 60).

The details of the beam-column sections are listed in Table 3 and depicted in Fig. 12.

Various cross-sections of the beam and column were defined as listed in Table 4 for use during the optimization process to minimize the weight of the structure and preserve the desired structural response under the applied loads.

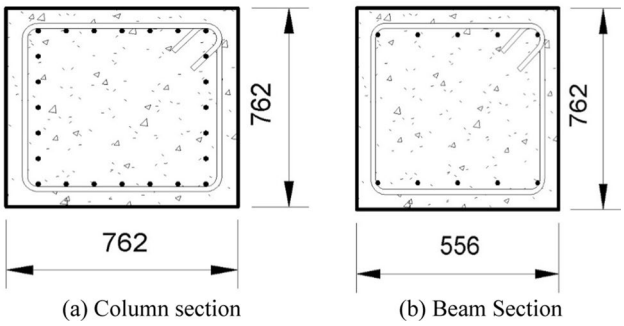


**Fig. 12** Details and dimensions of beam and column (mm) sections

For the optimization process, seven different ground motions were selected. The ground movement search criteria are displayed in Table 5, and the selected earthquakes, as shown in Table 6, were applied to the design according to the ASCE 7-10, for different intensities and periods. All the applied time-history data were scaled to match the target response rate.

## 7 Results and discussion

This section presents the results of the optimized design for the considered 12-storey structure equipped with damper devices, according to the performance-based design method, using the developed PSOGSA optimization technique.

### 7.1 Fitness function during the optimization process

Variations in the fitness function during the optimization process for the considered 12-storey structure using the PSOGSA method are shown in Fig. 13. The fitness function represented the formation of plastic hinges, the maximum displacements in the two orthogonal directions, and the maximum inter-storey drift for each time-history seismic analysis. The figure shows that the fitness function decreased and became stable within the first 100 iterations of the optimization process, and the convergency of optimization was successfully achieved by minimizing the fitness function in 269 iterations.

**Table 3** Details of beam-column sections for the considered structure (bare frame)

| Story | Beams | | | Columns | | |
|---|---|---|---|---|---|---|
| | Dimensions (m) | No. of reinforcement | Bar size (mm) | Dimensions (m) | No. of reinforcement | Bar size (mm) |
| 1–12 | 0.556 (w) × 0.762 (h) | 10 | 28 | 0.762 (w) × 0.762 (h) | 24 | 22 |

**Table 4** Various sections considered for beams and columns

| Columns dimensions (mm) | Beams dimensions (mm) |
|---|---|
| 500×500 | 450×500 |
| 510×510 | 450×510 |
| 520×520 | 450×520 |
| 540×540 | 450×540 |
| 550×550 | 500×550 |
| 560×560 | 600×560 |
| 580×580 | 600×580 |
| 590×590 | 580×590 |
| 600×600 | 580×600 |
| 610×610 | 600×610 |
| 620×620 | 580×620 |
| 640×640 | 580×640 |
| 660×660 | 580×660 |
| 680×680 | 600×680 |
| 690×690 | 600×690 |
| 700×700 | 600×700 |
| 720×720 | 600×720 |
| 740×740 | 600×740 |
| 750×750 | 600×750 |
| 762×762 | 556×762 |

**Table 5** Search criteria in PEER Ground Motion Database

| PEER ground motion database search criteria | Range |
|---|---|
| Magnitude Min | 6.5 |
| Magnitude Max | 7.5 |
| Rrup Min (km) | 10 |
| Rrup Max (km) | 30 |
| Rjb Min (km) | 10 |
| Rjb Max (km) | 30 |
| Vs30 Min (m/sec) | 360 |
| Vs30 Max (m/sec) | 760 |
| D9-95 Min (sec) | 15 |
| D9-95 Max (sec) | 60 |
| Scale Factor Min | 0.1 |

## 7.2 Weight of optimized structure

In this section, the details of the beams and columns, and the selected optimum vibration damper type and the specifications of the optimized structure by the developed PSOGSA algorithm are presented in Table 7. As can been seen from the results, the sizes of the sections for both the beams and columns were reduced in the optimized structure compared to the bare frame. Also, among all the considered vibration damping systems, the RBD1 device exhibited the best performance in dissipating the effect of the applied vibrations and satisfying the acceptance criteria for the performance-based design method. Therefore, it was selected as the optimum damper device for all the storeys during the optimization process. The location and configuration of the installed RBD1 damper devices in the optimized 12-storey structure are shown in Fig. 14.

Accordingly, the total weight of the concrete and steel materials for all the beam-column sections in the various floors of the considered 12-storey bare frame and the optimized structure are listed in Table 8. As can been from the results, the steel material that was used for the steel reinforcement was reduced by around 13% in storeys 4 to 12 in the optimized structure compared to the bare frame. However, there was a slight increase in the steel bars for the first 3 storeys as more strength was required for the implementation of the vibration damper devices.

Also, the results revealed that the total amount of concrete material for the optimized structure was noticeably reduced in the range of 47% to 34% for storeys 1 to 12, thereby indicating the efficiency of the developed PSOGSA optimization method in minimizing the overall weight of the structure from 4.98 tons to 2.85 tons (42% reduction) and reducing the construction cost of the structure through the implementation of an optimum vibration damping system that satisfied all the required acceptance criteria regarding the seismic response of the structure according to the performance-based design method. Although the optimization process resulted in small sections for the beams and columns, and a reduction of 13% in steel reinforcement for

**Table 6** Selected earthquake magnitudes

| Name | Magnitude | Maximum considered earthquake | Design-based earthquake |
|---|---|---|---|
| Cerro Prieto (1979) | 6.53 | MCE 1 | DBE 1 |
| Corinth (1981) | 6.6 | MCE 2 | DBE 2 |
| Coyote Lake Dam-Southwest Ab. (1989) | 6.93 | MCE 3 | DBE 3 |
| Fortuna—Fortuna Blvd (1992) | 7.01 | MCE 4 | DBE 4 |
| Joshua Tree (1992) | 7.28 | MCE 5 | DBE 5 |
| Morongo Valley Fire Station (1992) | 7.28 | MCE 6 | DBE 6 |
| Sunland—Mt Gleason Ave (1994) | 6.69 | MCE 7 | DBE 7 |

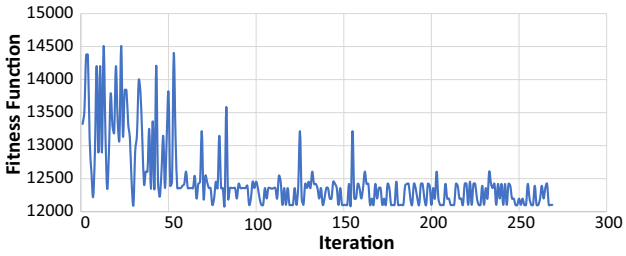


**Fig. 13** Objective function during the optimization process

the 4th to 12th storeys, however, relatively large section sizes for the beams and columns for the first-to-third floors were determined. Also, the optimization algorithm calculated a slightly higher amount of reinforcement (steel bars) for the first three storeys in comparison to the initial design. This was because the implementation of damper devices in the structure to control and minimize the movements of the structure through the dissipation of induced structural vibrations caused the generation of noticeable shear forces in the

**Table 7** Details of the sections for the beams and columns and selected optimum damper type and specifications in the optimized structure

| Optimum structural section | | | | | | | |
|---|---|---|---|---|---|---|---|
| Storey level | Beams | | | Columns | | | Optimized Damper |
| | Dimensions (m) | No. of Steel Reinforcement | Bar Size (mm) | Dimensions (m) | No. of Steel Reinforcement | Bar Size (mm) | |
| 1–3 | 0.6×0.7 | 10 | 28 | 0.7×0.7 | 24 | 32 | RBD 1 |
| 4–12 | 0.45×0.51 | 10 | 25 | 0.51×0.51 | 24 | 22 | RBD 1 |

| Optimum damper types and properties | | | |
|---|---|---|---|
| Storey level | Optimum damper type | Stiffness (KN/mm) | Damping (KN×s/m) |
| 1–12 | RBD1 | 30.315 | 108.35 |

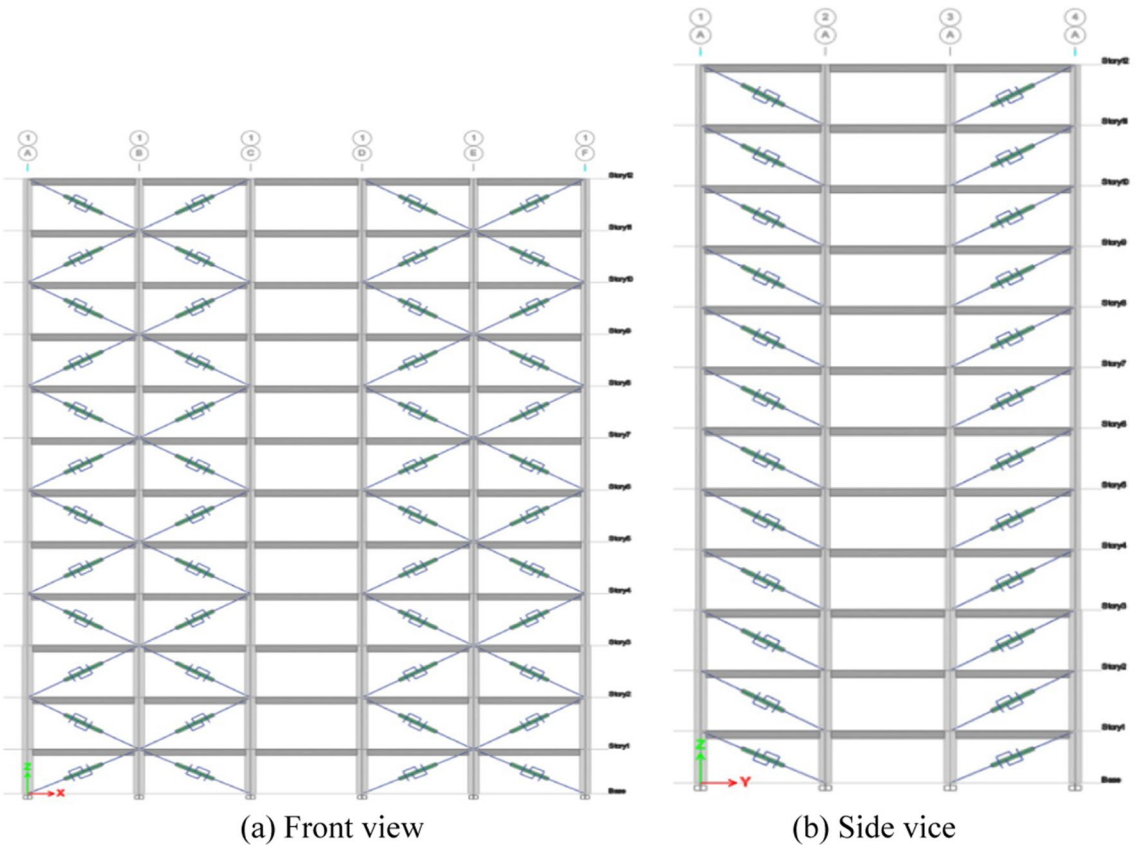


**Fig. 14** Location and configuration of installed RBD1 damper devices in the optimized 12-storey structure

**Table 8** Weight of bare frame and optimized structure with damper device

| Storey | Bare frame | | Optimized structure | | Reduction of Steel material (%) | Reduction of concrete metrical (%) | Overall reduction (%) |
|---|---|---|---|---|---|---|---|
| | Steel (ton) | Concrete (ton) | Steel (ton) | Concrete (ton) | | | |
| 1 | 19.74 | 396.65 | 20.91 | 206.74 | −5.95 | 47.88 | 45.33 |
| 2 | 20.78 | 396.65 | 22.59 | 206.74 | −8.75 | 47.88 | 45.06 |
| 3 | 20.78 | 396.65 | 22.59 | 206.74 | −8.75 | 47.88 | 45.06 |
| 4 | 20.77 | 396.65 | 18.04 | 206.74 | 13.14 | 47.88 | 46.15 |
| 5 | 20.77 | 396.65 | 18.04 | 206.74 | 13.14 | 47.88 | 46.15 |
| 6 | 20.77 | 396.65 | 18.04 | 206.74 | 13.14 | 47.88 | 46.15 |
| 7 | 20.77 | 396.65 | 18.04 | 206.74 | 13.14 | 47.88 | 46.15 |
| 8 | 20.77 | 396.65 | 18.04 | 206.74 | 13.14 | 47.88 | 46.15 |
| 9 | 20.77 | 396.65 | 18.04 | 206.74 | 13.14 | 47.88 | 46.15 |
| 10 | 20.77 | 396.65 | 18.04 | 259.35 | 13.14 | 34.61 | 33.55 |
| 11 | 20.77 | 396.65 | 18.04 | 259.35 | 13.14 | 34.61 | 33.55 |
| 12 | 20.77 | 376.23 | 18.04 | 242.12 | 13.14 | 35.65 | 34.47 |

sections of beams and columns, thereby transferring all the shear forces to the base of the structure, and causing the first few storeys to carry more accumulated forces compared to the higher storeys. Therefore, the optimization output for the structure furnished with damper devices was more obvious for the members in the middle and higher storeys compared to the few first storeys.

### 7.3 Displacement results

The data on seven earthquake records were considered, according to the ASCE 7-10 (Minimum Design Loads and Associated Criteria for Buildings and Other Structures, 2017) to determine the seismic response of the structure. Based on Chapter 18, Sect. 18.2.2.2 on the Seismic Design Requirements for Structures with Damping Systems (ASCE 7-16), the MCER ground motions should consist of not less than seven earthquake acceleration data. Therefore, using seven or more motions, the mean results can be used for the evaluation of the seismic response of a structure. Therefore, in this study, the seven earthquake acceleration records on the Design-Basis Earthquake (DBE) and Maximum Considered Earthquake (MCE) were selected based on the site location of the structure, and the conditions that were scaled to fit a continuum range of 5% damped acceleration response, consistent with Sect. 11.4.5 of the ASCE 7, 2010.

Accordingly, the considered structure was subjected to the seven earthquake acceleration records at both the DBE and MCE levels, and a non-linear time-history analysis was conducted for each seismic record. Since the structure was oscillating sideways, therefore, movements to the right and left were considered as positive and negative displacements, respectively. To design the structure for critical conditions, the positive maximum displacement (Dmaxp) and the negative maximum displacement (Dmaxn) of the structural time-history response for all seven earthquakes at the DBE and MCE levels were considered for the bare frame and optimized frame, as shown in Fig. 15. Also, the mean for the positive and negative time-history displacements for each seismic record was calculated for both the bare frame and the optimized frame, as listed in Table 9, and shown in Fig. 16.

Eventually, the mean displacement and variance for the structural response under the applied seven earthquakes at the DBE and MCE levels for the bare frame and optimized frame were calculated, and are presented in Table 10. The results revealed that the implementation of the structural design using the developed optimization method was able to successfully reduce the seismic response of the structure by about 41.3% for the Design-Basis Earthquake, and 41.8% for the Maximum Considered Earthquake in comparison to the bare frame.

### 7.4 Results of storey drift

The overall maximum inter-storey drift along the height of the structure due to the application of the seven types of earthquake records at the DBE and MCE levels for the initial and optimized designs of the structure equipped with damper devices is shown in Fig. 17.

According to the ASCE 7-10, Sect. 12.12.1, the allowable storey drift is 2%. Therefore, as can be seen from the graphs, the inter-storey drift for the MCE level exceeded the allowable movement in both the X and Y-directions in the preliminary designed structure based on the ACI 318-14. However, in the optimized design of the structure, the inter-storey drift was within the range for the same MCE level.

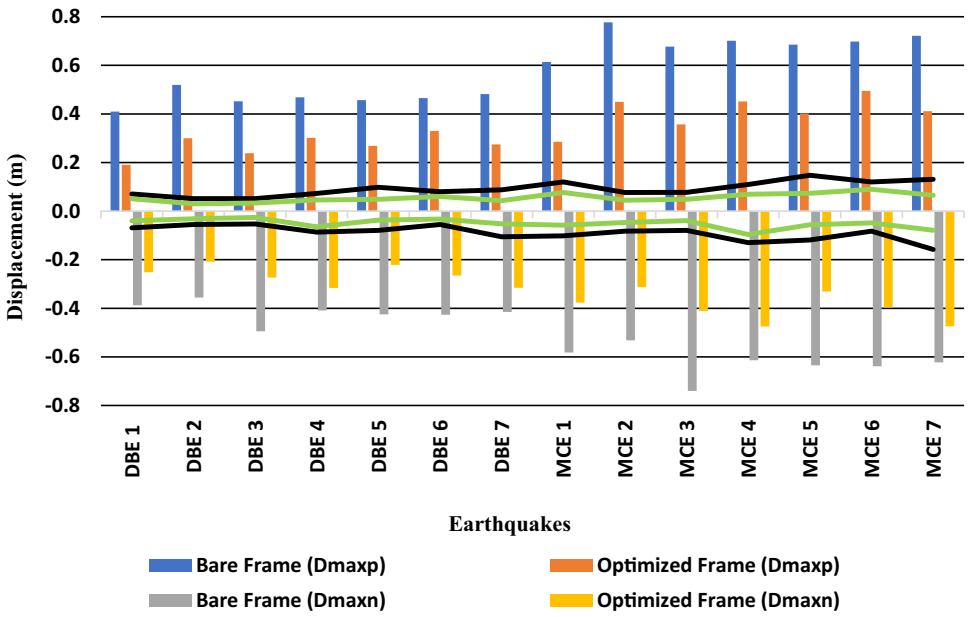


**Fig. 15** Maximum positive and negative displacements, means and variances for the maximum displacement response of the bare and optimized structures for all seven earthquakes at the DBE and MCE levels

**Table 9** Means and variances for maximum displacement response of bare and optimized structures for all seven earthquakes at the DBE and MCE levels

| Earthquakes | DBE Level | | | | MCE Level | | | |
|---|---|---|---|---|---|---|---|---|
| | Bare Frame | | Optimized Frame | | Bare Frame | | Optimized Frame | |
| | Mean Dis (m) | Variance | Mean Dis (m) | Variance | Mean Dis (m) | Variance | Mean Dis (m) | Variance |
| Cerro Prieto (1979) | 0.0696 | 0.00577 | 0.0454 | 0.00220 | 0.1111 | 0.01294 | 0.0672 | 0.00494 |
| Corinth (1981) | 0.0531 | 0.00649 | 0.0307 | 0.00212 | 0.0796 | 0.01457 | 0.0460 | 0.00476 |
| Coyote Lake Dam-Southwest Ab. (1989) | 0.0523 | 0.00714 | 0.0295 | 0.00216 | 0.0782 | 0.01598 | 0.0440 | 0.00486 |
| Fortuna—Fortuna Blvd (1992) | 0.0798 | 0.00710 | 0.0552 | 0.00390 | 0.1196 | 0.01595 | 0.0829 | 0.00879 |
| Joshua Tree (1992) | 0.0888 | 0.00929 | 0.0430 | 0.00233 | 0.1331 | 0.02089 | 0.0645 | 0.00523 |
| Morongo Valley Fire Station (1992) | 0.0675 | 0.00788 | 0.0462 | 0.00337 | 0.1013 | 0.01768 | 0.0691 | 0.00758 |
| Sunland—Mt Gleason Ave (1994) | 0.0965 | 0.00714 | 0.0478 | 0.00684 | 0.1444 | 0.03116 | 0.0718 | 0.01550 |

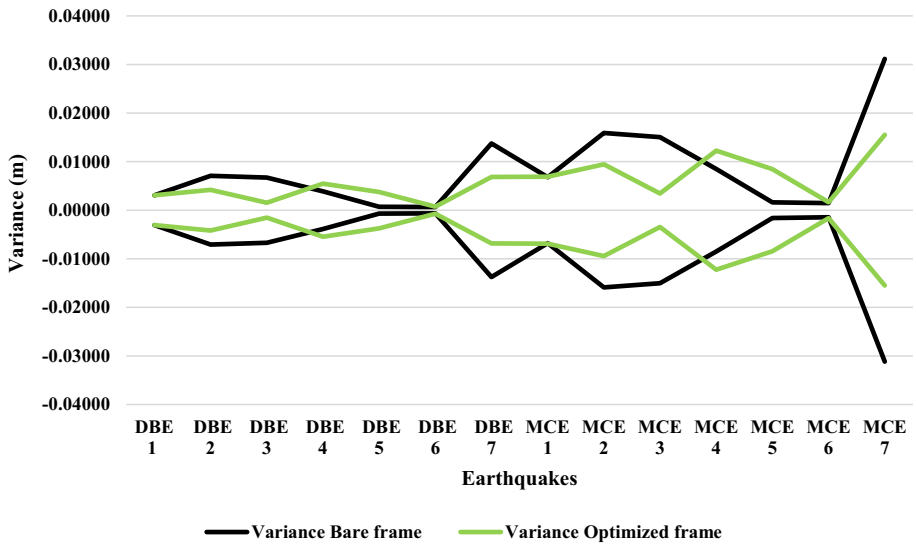


**Fig. 16** Variance of positive and negative time-history displacements of the structure for seven earthquakes at the DBE and MCE levels

**Table 10** Means and variances of displacement response for bare and optimized frames subjected to seven earthquakes at the DBE and MCE levels

| Earthquakes | Mean displacement (m) | Reduction (%) | Variance |
|---|---|---|---|
| Bare frame (DBE) | 0.0725 | – | 0.00726 |
| Optimized frame (DBE) | 0.0425 | 41.3 | 0.00259 |
| Bare frame (MCE) | 0.1096 | – | 0.01628 |
| Optimized frame (MCE) | 0.0637 | 41.8 | 0.00582 |

Overall, the results indicated that the inter-storey drift in the optimized design structure equipped with a vibration dissipation system was highly reduced in the range of 34% to 47% for both the DBE and MCE records in comparison to the inter-storey drift for the preliminary designed structure, as presented in Table 11. Therefore, it was deduced that the developed PSOGSA method effectively reduced the inter-storey drift of the structure using the optimum design of the structure and the type and properties of the optimum structural damping system.

### 7.5 3D interaction yield surface of P-M2-M3 hinges for concrete structure

The moment-rotation curve for a P-M2-M3 hinge is a three-dimensional backbone relationship which is used to describe the post-yield behaviour of a beam-column element subjected to combined axial forces and biaxial bending moments around the local axis in 2–2 and 3–3. Therefore, this interaction curve is implemented to capture the actual non-linear behaviour of RC beams or columns subjected to external forces, and to identify the occurrence of any plastic hinges when the internal force of the members is beyond their capacity (outside of the yield surface).

Figure 18 shows the 3D interaction yield surface and internal force position (force generated during application) in the corner column at the first storey of the preliminary designed structure and optimized design structure for all the various combinations of P, M2 and M3 (axial force, moment around 2–2 axes, moment around 3–3 axes) during the optimization process.

As can be seen from the results, the optimization process managed to shift 100% of the points representative of the internal force of the structural members from the outside of the three-dimensional P-M2-M3 yield surface (plastic or yielding zone) to the inside of the curve (elastic zone) by implementing the optimized design and utilizing the optimum damper devices simultaneously with a reduction in the total weight of the structure (Fig. 18).

Similarly, as can be seen in Fig. 18, about 76%, 59%, and 66% of the hinges in the same corner column (on the first floor) were shifted from out of the yield surface for the M2–M3, P–M2 and P–M3, respectively to the elastic zone (inside of the curve) during the optimization of the structure equipped with damper devices.

Therefore, these results confirmed that the developed PSOGSA algorithm was able to effectively optimize the seismic design of the structure by utilizing a vibration damping system to minimize damage in the structural members due to an applied earthquake load by satisfying the acceptance criteria for the performance-based design method.

### 7.6 Results on occurrence of plastic hinges

The overall number of occurrences of plastic hinges in the structural members and also the percentage of reduction in the occurrence of plastic hinges during the application of the seven types of DBE and DBE accelerations that were considered in the various optimization iterations are shown in Fig. 20, while the details are listed in Table 12 for the bare frame and optimized structure.

As can be seen from the results of the bare frame (structure before optimization and without vibration dissipation system) in Fig. 19a, and in Table 12 (for the DBE and MCE), only a few plastic hinges were observed in the columns in some of the applied earthquake records at the DBE level for the bare frame in the performance of the IO–LS and LS–CP. However, the number of plastic hinges that were formed in the columns of the bare frame for the various applied MCE records was in range of 10 to 22 plastic hinges for the performance of the LS-CP and 20 to 78 plastic hinges for the performance of the LS-IO. Therefore, it was revealed that the bare frame was partially damaged at the DBE level, but for the considered MCE, the structure was highly vulnerable in the LS–CP and almost collapsed in the LS-IO.

However, the results presented in Table 12 showed that there were no plastic hinges in the structural members of the optimized structure at both the DBE and MCE levels for the performance of all the various IO–LS and LS–CP of the structure, and as can be seen in Fig. 19b, the overall percentage of reduction in the formation of plastic hinges in the structure was 100% for the seven earthquake records that were applied at the DBE and MCE levels, respectively. Therefore, it was revealed that the developed POSGSA optimization method was able to successfully optimize the seismic design of the 12-storey structure throughout the optimization iterations by utilizing an appropriate vibration damper device to prevent the formation of any plastic hinges in the structural members for both the MCE and DBE seismic excitations.

Additionally, a non-linear time-history analysis was carried out for the MCE records using predicted structural strengths to survive trembling, as described in Section C1.3.1 of the ASCE 7–10, with decreasing likelihood (up

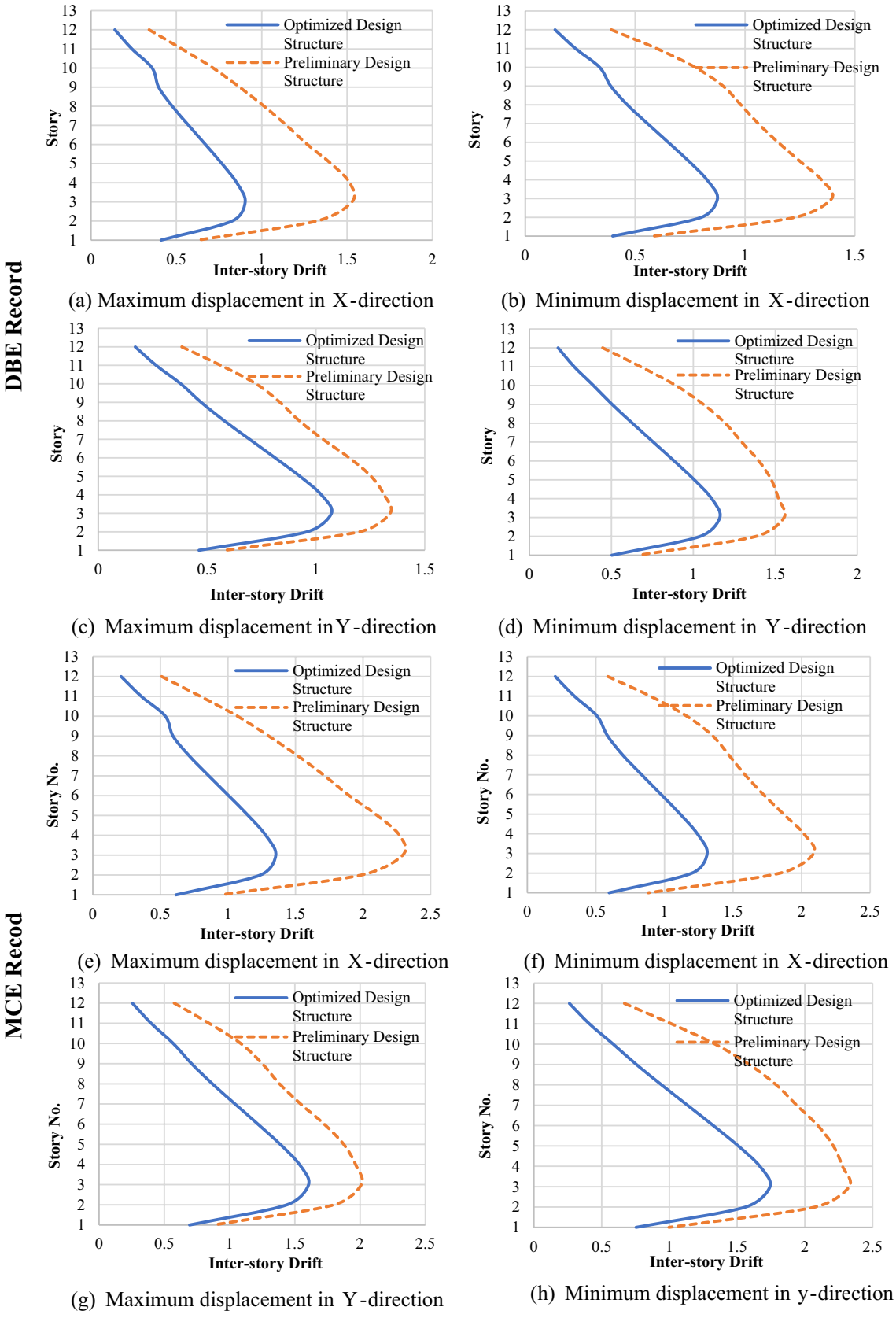


**Fig. 17** Inter-storey drift along height for the preliminary design structure and optimized design structure for DBE and MCE records

**Table 11** Inter-storey drift deduction (%) in the optimized design structure in comparison to the preliminary designed structure

| DBE earthquakes level | | | | MCE earthquakes level | | | |
|---|---|---|---|---|---|---|---|
| Drift deduction in *X*-direction | | Drift deduction in *Y*-direction | | Drift deduction in *X*-direction | | Drift deduction in *Y*-direction | |
| Max | Min | Max | Min | Max | Min | Max | Min |
| 47.54% | 47.24% | 33.95% | 40.66% | 47.54% | 47.22% | 33.93% | 40.62% |

from 10% of complete and partial collapse). Then, according to the code statement, the optimized structure would be on the safe side as there would be no failure in any structural members.

Therefore, it could be concluded that the developed PSOGSA algorithm successfully optimized the design of the structure equipped with damper devices according to the performance-based design method to protect the structure from any seismic damage at different earthquake levels (DBE and MCE) and within the range of the operational level of the structure (LS-IO).

## 7.7 Base reaction for design-basis earthquake and maximum considered earthquake

The effects of the vibration dissipation devices installed in the optimized frame on the base reaction, including the shear forces and bending moments, during a seismic excitation were studied for both a Design-Basis Earthquake and Maximum Considered Earthquake.

### 7.7.1 Base reaction in the structure for a design-basis earthquake

The analysis results demonstrated that of the overall base reaction due to the applied DBE decreased when the structure was equipped with dampers, as shown in Table 13, for the bare frame and optimized structure, respectively.

The results illustrated that the dampers had a noteworthy effect on the base shear forces; however, there was not much effect on the moment forces. This reduction in the maximum base shear in the horizontal *X*-direction was about 27%, 39%, 34%, 9%, 26%, 30%, and 3% for the DB1 to DB7 earthquakes, respectively. Also, the minimum base shear in the same direction (*X*), was reduced by around 48%, 23%, 37%, 25%, 32%, 18%, and 33% in the optimized structure equipped with the selected damper device for DBE1 to DBE7, respectively.

Likewise, the maximum and minimum shear forces in the horizontal *Y*-direction were reduced in the optimized structure in the range of 13 to 34% and 4 to 25%, respectively.

In contrast, there was not much effect on the base moment in the optimized structure equipped with damper devices and the bare frame.

The noticeable reduction in the base shear forces was due to the action of the implemented vibration damping system in the structure, which absorbed a part of the applied vibration energy and dissipated its effect in the structural response.

### 7.7.2 Base reaction in the structure for maximum considered earthquake

The results of the overall base reaction for the bare frame and optimized structure under the applied MCE are presented in Table 14, respectively.

The results illustrated that the maximum base shear in the horizontal X-direction in the optimized structure was reduced by about 27%, 39%, 34%, 9.3%, 26%, 30%, and 3% for the applied MCE1 to MCE7, respectively. Similarly, the reduction for the minimum base shear in the same direction was 49%, 23%, 36%, 25%, 32%, 18%, and 32% for MCE1 to MCE7, respectively.

Accordingly, the same reductions were observed for the minimum and maximum base shear in the Y-direction in the range of 13 to 34% and 4 to 25%, respectively for the applied MCE due to the implementation of the optimized design of the structure and the vibration dissipation system. However, again, there was not much effect on the moment forces.

## 7.8 Demand-To-Capacity ratio of the columns

The demand-to-capacity ratio of the columns for the bare frame compared to the optimized structure was evaluated by considering the effects of the vibration dissipation device installed in the frame during the Design-Basis Earthquake and the Maximum Considered Earthquake.

### 7.8.1 Demand-to-capacity ratio of the columns for design-basis earthquake

The results revealed that the overall demand-to-capacity ratio for the columns decreased in the optimized structure equipped with dampers, as shown in Table 15 and Fig. 20. The results illustrated that the implementation of damper devices in the structure had a noteworthy effect on the capacity of the structure. This corresponded with a decrease of about 99.8%, 98.7%, 99.5%, 99.4%, 99.5%, 99.99%, and 99.99% in the demand-to-capacity ratio of the columns

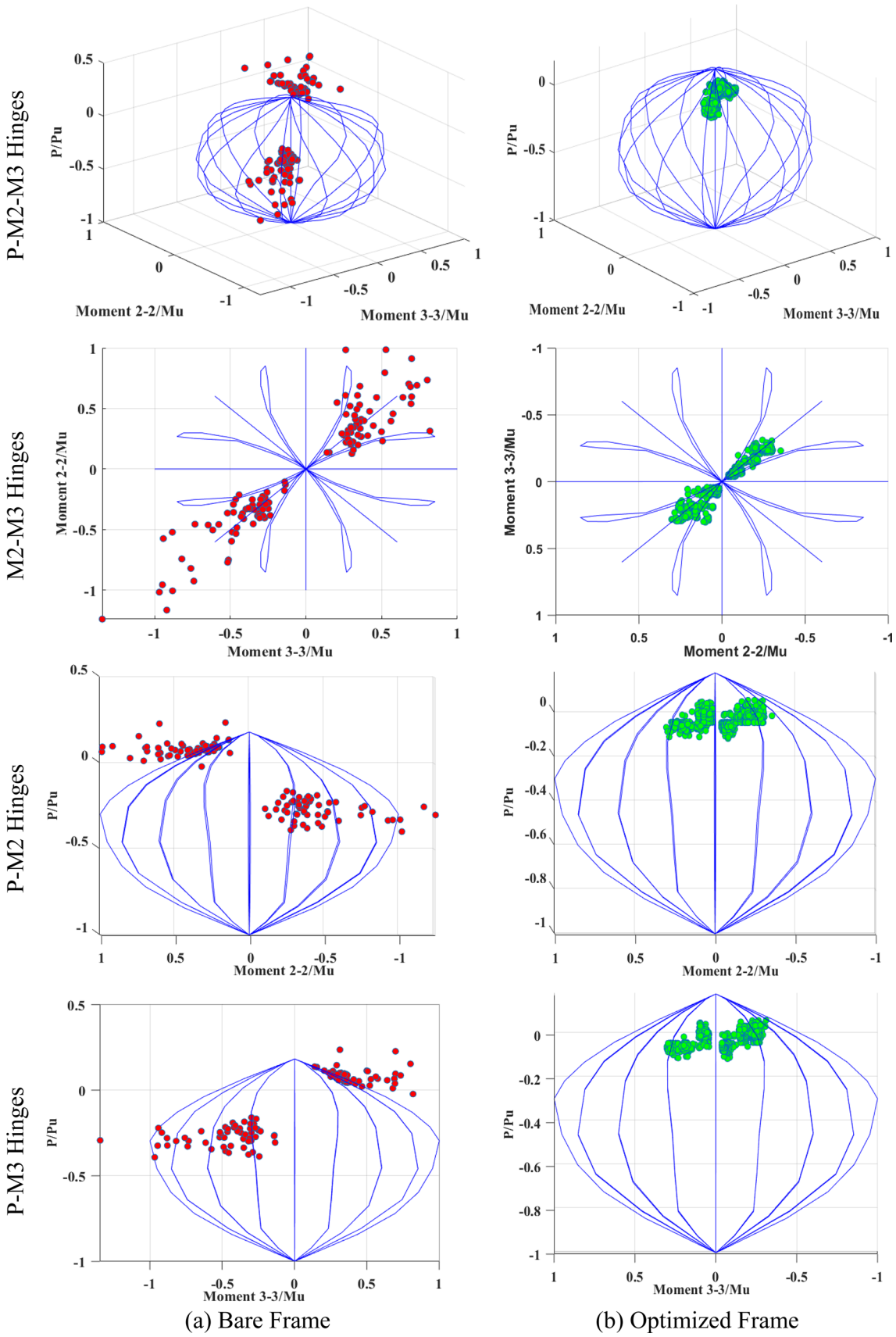


**Fig. 18** The 3D interaction yield surface for the bare and optimized frames

**Table 12** Number of plastic hinges formed at the various performance levels for the considered DBE and MCE seismic records in the bare and optimized frames

| Structure | Earthquake | Applied earthquake record | Plastic hinges numbers according to performance levels | | | | | | | |
|---|---|---|---|---|---|---|---|---|---|---|
| | | | Beams | | | | Columns | | | |
| | | | < IO | IO—LS | LS–CP | > CP | < IO | IO–LS | LS–CP | > CP |
| Bare Frame | DBE Level | DBE 1 | 456 | 0 | 0 | 0 | 567 | 0 | 2 | 0 |
| | | DBE 2 | 456 | 0 | 0 | 0 | 567 | 3 | 5 | 0 |
| | | DBE 3 | 456 | 0 | 0 | 0 | 567 | 0 | 2 | 0 |
| | | DBE 4 | 456 | 0 | 0 | 0 | 567 | 1 | 4 | 0 |
| | | DBE 5 | 456 | 0 | 0 | 0 | 545 | 2 | 3 | 0 |
| | | DBE 6 | 456 | 0 | 0 | 0 | 567 | 0 | 0 | 0 |
| | | DBE 7 | 456 | 0 | 0 | 0 | 509 | 1 | 1 | 0 |
| Bare Frame | MCE Level | MCE 1 | 456 | 0 | 0 | 0 | 501 | 31 | 15 | 20 |
| | | MCE 2 | 456 | 0 | 0 | 0 | 491 | 34 | 22 | 26 |
| | | MCE 3 | 456 | 0 | 0 | 0 | 524 | 24 | 10 | 17 |
| | | MCE 4 | 456 | 0 | 0 | 0 | 447 | 78 | 18 | 24 |
| | | MCE 5 | 456 | 0 | 0 | 0 | 525 | 25 | 14 | 17 |
| | | MCE 6 | 456 | 0 | 0 | 0 | 518 | 20 | 11 | 18 |
| | | MCE 7 | 456 | 0 | 0 | 0 | 489 | 33 | 19 | 26 |
| Optimized Frame | DBE Level | DBE 1 | 456 | 0 | 0 | 0 | 567 | 0 | 0 | 0 |
| | | DBE 2 | 456 | 0 | 0 | 0 | 567 | 0 | 0 | 0 |
| | | DBE 3 | 456 | 0 | 0 | 0 | 567 | 0 | 0 | 0 |
| | | DBE 4 | 456 | 0 | 0 | 0 | 567 | 0 | 0 | 0 |
| | | DBE 5 | 456 | 0 | 0 | 0 | 545 | 0 | 0 | 0 |
| | | DBE 6 | 456 | 0 | 0 | 0 | 567 | 0 | 0 | 0 |
| | | DBE 7 | 456 | 0 | 0 | 0 | 509 | 0 | 0 | 0 |
| Optimized Frame | MCE Level | MCE 1 | 456 | 0 | 0 | 0 | 567 | 0 | 0 | 0 |
| | | MCE 2 | 456 | 0 | 0 | 0 | 567 | 0 | 0 | 0 |
| | | MCE 3 | 456 | 0 | 0 | 0 | 567 | 0 | 0 | 0 |
| | | MCE 4 | 456 | 0 | 0 | 0 | 567 | 0 | 0 | 0 |
| | | MCE 5 | 456 | 0 | 0 | 0 | 567 | 0 | 0 | 0 |
| | | MCE 6 | 456 | 0 | 0 | 0 | 567 | 0 | 0 | 0 |
| | | MCE 7 | 456 | 0 | 0 | 0 | 567 | 0 | 0 | 0 |

for immediate occupancy, life safety, and collapse prevention operational levels for the considered DBE 1 to DBE 7, respectively.

#### 7.8.2 Demand-to-capacity ratio of the columns for maximum considered earthquake

The results of the overall demand-to-capacity ratio of the columns in the bare frame and optimized structure are presented in Table 16 and Fig. 21.

As can be seen from the results, the utilization of damper devices in the optimized structure led to a decrease in the demand-to-capacity ratio of the columns of about 98.3%, 98.5%, 99.8%, 97.4%, 99.7%, 99.4%, and 98.3% for the considered MCE1 to MCE 7, respectively for immediate occupancy, life safety and collapse prevention operational levels.

Therefore, the results proved that the use of the optimized design with the damper devices had a noteworthy effect on the capacity of the structure.

## 8 Validation of developed PSOGSA algorithm through other optimization methods

To validate the results of the PSOGSA optimization algorithm, it was applied for the optimization of a 12-storey RC structure, and the results in terms of a reduction in the maximum displacement response were investigated. The same process was performed using other optimization techniques such as the genetic algorithm (GA), ant colony optimization (ACO) and particle swarm optimization (PSO), and THE

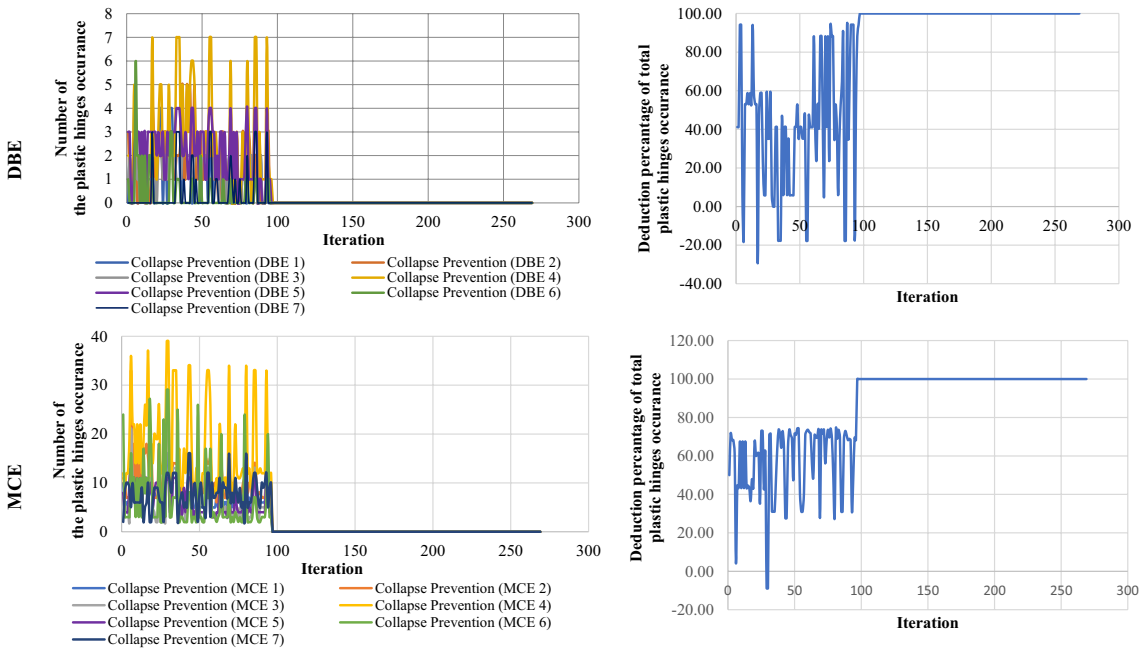


(a) Number of plastic hinges formed in the columns of the bare frame under the applied earthquake records

(b) Overall deduction percentage of the occurrence of plastic hinges during the optimization process

**Fig. 19** Results on the formation of plastic hinges during the optimization process

results were compared to the output of the PSOGSA optimization method.

Then, the optimization outputs were evaluated with respect to the fitness function, plastic hinge development in the structural members, and maximum displacements during earthquake excitations at both the DBE and MCE levels, as demonstrated in detail as follows:

## 8.1 Fitness function

Figure 22 shows the decrease in the overall fitness function optimization process. Furthermore, the fitness was plotted in respect of the occurrence of plastic hinges, maximum displacement in the two applied orthogonal time-history data, the maximum inter-storey drift, and the weight of the concrete.

Additionally, the PSOGSA found the optimal solution after around 250 iterations in comparison with the other algorithms that found it after 900, 900, and 650 iterations for the GA (genetic algorithm), ACO (ant colony optimization), and PSO (particle swarm optimization), respectively. Therefore, much less computational power and time were required to finish the optimization process.

## 8.2 Plastic hinges

The reduction in the formation of plastic hinges in the structural members under earthquake excitations at the DBE and MCE levels for the optimized structure for all optimization iterations using various optimization methods is depicted in Fig. 23.

As can be seen from the graph in Fig. 23, both the PSOGSA and GA methods resulted in the greatest reduction of 88.2% in the formation of plastic hinges in the beams and columns under the DBE, while the developed PSOGSA algorithm was able to obtain the best design within just 269 iterations in comparison to the GA method with 900 iterations. Two other methods, namely the PSO and AC methods, were able to reduce the occurrence of plastic hinges to 64.7% and 41.1% within 650 and 900 iterations, respectively. These results indicated the efficiency of the developed PSOGSA method in obtaining the maximum reduction of plastic hinges in the structural members via a minimum computation time and effort in comparison to other conventional optimization methods.

The same graph corresponding to the MCE level in Fig. 23 also revealed that all the optimization methods resulted in a reduction of 73% in the occurrence of plastic hinges in the structural members. Hence, the PSOGSA algorithm produced results after only 269 iterations, thereby proving the very fast convergency of this technique in comparison to the other methods, which obtained an output after 650 and 900 iterations.

**Table 13** Base reaction in the bare and optimized frames for DBE

| Structure | Applied earthquake record | Step type | Shear force (X) (kN) | Shear force (Y) (kN) | Moment (X) (kN.m) | Moment (Y) (kN.m) |
|---|---|---|---|---|---|---|
| Bare Frame | DBE 1 | Max | 11,140.51 | 9724.422 | 1,323,192 | − 1,295,912 |
| | DBE 1 | Min | − 12,066.2 | − 12,094.9 | 687,553.7 | − 1,967,057 |
| | DBE 2 | Max | 11,134.82 | 13,050.48 | 1,288,436 | − 1,292,806 |
| | DBE 2 | Min | − 14,416.5 | − 11,094.7 | 589,578.4 | − 2,030,004 |
| | DBE 3 | Max | 13,408.69 | 12,463.99 | 1,184,021 | − 1,228,413 |
| | DBE 3 | Min | − 12,223.6 | − 7296.98 | 608,137.5 | − 1,971,829 |
| | DBE 4 | Max | 11,406.86 | 13,040.59 | 1,356,635 | − 1,284,550 |
| | DBE 4 | Min | − 13,170.5 | − 13,350.3 | 589,291.6 | − 1,998,374 |
| | DBE 5 | Max | 11,068.53 | 9698.496 | 1,335,897 | − 1,298,347 |
| | DBE 5 | Min | − 12,632.3 | − 12,542.3 | 686,002.4 | − 1,981,245 |
| | DBE 6 | Max | 12,211.41 | 11,516.93 | 1,315,161 | − 1,264,195 |
| | DBE 6 | Min | − 13,284.5 | − 11,847 | 637,087.4 | − 2,004,642 |
| | DBE 7 | Max | 10,653.12 | 13,254.46 | 1,110,463 | − 1,308,651 |
| | DBE 7 | Min | − 13,144.5 | − 4983.09 | 581,529.9 | − 2,000,390 |
| Optimized Frame | DBE 1 | Max | 8166.085 | 8438.872 | 1,246,118 | − 1,376,637 |
| | DBE 1 | Min | − 6260.57 | − 9292.69 | 722,071 | − 1,800,075 |
| | DBE 2 | Max | 6762.186 | 10,810.13 | 1,237,368 | − 1,425,389 |
| | DBE 2 | Min | − 11,018.1 | − 10,626.1 | 650,964 | − 1,906,377 |
| | DBE 3 | Max | 8821.712 | 9219.588 | 1,165,684 | − 1,355,648 |
| | DBE 3 | Min | − 7730.36 | − 6648.12 | 697,724.5 | − 1,844,044 |
| | DBE 4 | Max | 10,344.56 | 8594.643 | 1,357,404 | − 1,317,926 |
| | DBE 4 | Min | − 9791.61 | − 13,947 | 716,241.4 | − 1,896,259 |
| | DBE 5 | Max | 8133.212 | 11,922.73 | 1,255,175 | − 1,406,043 |
| | DBE 5 | Min | − 8560.18 | − 9713.03 | 666,940.3 | − 1,864,674 |
| | DBE 6 | Max | 8499.672 | 9187.143 | 1,228,622 | − 1,370,061 |
| | DBE 6 | Min | − 10,827.3 | − 8805.98 | 697,472.3 | − 1,931,478 |
| | DBE 7 | Max | 10,334.44 | 12,224.53 | 1,137,830 | − 1,320,702 |
| | DBE 7 | Min | − 8832.3 | − 6761.83 | 611,029.3 | − 1,872,639 |

### 8.3 Maximum displacements

The percentage reductions in the Maximum Positive Displacement (movement to the right side) and Maximum Negative Displacement (movement to the left side) in the X and Y-directions in the various iteration steps of the different optimization techniques for the structure under the Design-Basis Earthquake (DBE) and Maximum Considered Earthquake (MCE) are listed in Table 17 and presented in Figs. 24 and 25.

As can be seen from the results, the PSOGSA and GA methods produced a maximum reduction of maximum displacements at both the DBE and MCE levels in the range of 41% ~ 43% in the *X*-direction and 23% to 27% in the *Y*-direction (perpendicular to the *X*-direction), while the PSO and ACO methods obtained maximum displacement reductions in the range of 38% to 43% in the *X*-direction and 24% to 27% in the *Y*-direction.

However, the results indicated that the PSOGSA method obtained the optimum point at an earlier stage after 269 iterations, while the PSO method reached the optimum point after 650 iterations, and both the GA and AC techniques had to attempt 900 iterations to complete the process.

Therefore, this proved the remarkable capability and advantages of the developed PSOGSA method to obtain an optimization convergency in a very short time compared to other similar methods, thereby leading to significant savings in computation time and cost. This advantage would be even more significant for the optimization of mega structures, high-rise buildings, and towers, which require strong and expensive computational facilities to process the mathematics and calculations for the optimization of structures furnished with damper devices.

**Table 14** Base reaction in the bare and optimized frames for MCE

| Structure | Applied earthquake record | Step type | Shear force (X) (kN) | Shear force (Y) (kN) | Moment (X) (kN.m) | Moment (Y) (kN.m) |
|---|---|---|---|---|---|---|
| Bare Frame | MCE 1 | Max | 16,735.77 | 14,598.99 | 1,498,126 | − 1,134,834 |
| | MCE 1 | Min | − 18,093.2 | − 18,089.6 | 545,892.4 | − 2,142,096 |
| | MCE 2 | Max | 16,663.86 | 19,552.76 | 1,446,287 | − 1,131,975 |
| | MCE 2 | Min | − 21,520.7 | − 16,594.2 | 400,022.1 | − 2,233,695 |
| | MCE 3 | Max | 20,038.29 | 18,676.76 | 1,290,706 | − 1,036,446 |
| | MCE 3 | Min | − 18,302.9 | − 10,934.2 | 427,741.6 | − 2,148,491 |
| | MCE 4 | Max | 17,107.04 | 19,496.39 | 1,546,553 | − 1,118,589 |
| | MCE 4 | Min | − 19,712.6 | − 19,907.8 | 400,832.1 | − 2,188,001 |
| | MCE 5 | Max | 16,499.37 | 14,548.96 | 1,518,227 | − 1,142,196 |
| | MCE 5 | Min | − 18,923.3 | − 18,793.3 | 543,972.9 | − 2,162,827 |
| | MCE 6 | Max | 18,255.79 | 17,282.46 | 1,486,636 | − 1,089,680 |
| | MCE 6 | Min | − 19,920.4 | − 17,731 | 470,435 | − 2,198,476 |
| | MCE 7 | Max | 15,973.96 | 19,889.38 | 1,178,323 | − 1,154,753 |
| | MCE 7 | Min | − 19,663.6 | − 7393.36 | 387,070.2 | − 2,190,747 |
| Optimized Frame | MCE 1 | Max | 12,241.6 | 12,661.26 | 1,383,836 | − 1,256,925 |
| | MCE 1 | Min | − 9393.72 | − 13,923.4 | 598,147.3 | − 1,891,932 |
| | MCE 2 | Max | 10,136.17 | 16,218.19 | 1,370,777 | − 1,330,006 |
| | MCE 2 | Min | − 16,535.9 | − 15,925.7 | 491,487 | − 2,051,558 |
| | MCE 3 | Max | 13,231.19 | 13,833.48 | 1,263,629 | − 1,225,253 |
| | MCE 3 | Min | − 11,592.6 | − 9970.64 | 561,581.5 | − 1,957,732 |
| | MCE 4 | Max | 15,515.36 | 12,899.84 | 1,550,580 | − 1,168,606 |
| | MCE 4 | Min | − 14,672.6 | − 20,897.9 | 589,257.2 | − 2,035,723 |
| | MCE 5 | Max | 12,167.02 | 17,860.21 | 1,397,585 | − 1,301,847 |
| | MCE 5 | Min | − 12,823.1 | − 14,559.1 | 515,819.7 | − 1,988,236 |
| | MCE 6 | Max | 12,736.31 | 13,786.28 | 1,357,710 | − 1,247,161 |
| | MCE 6 | Min | − 16,242.7 | − 13,195.3 | 561,181.4 | − 2,088,968 |
| | MCE 7 | Max | 15,499.53 | 18,342.03 | 1,220,657 | − 1,172,857 |
| | MCE 7 | Min | − 13,240.7 | − 10,101.5 | 431,536.4 | − 2,000,459 |

**Table 15** Demand-to-capacity ratio in the columns in bare and optimized frames for DBE

| Structure | Earthquake | Immediate occupancy | Life safety | Collapse prevention |
|---|---|---|---|---|
| Bare Frame | DBE 1 | 2.899 | 0.775 | 0.553 |
| | DBE 2 | 0.941 | 0.252 | 0.18 |
| | DBE 3 | 1.568 | 0.419 | 0.299 |
| | DBE 4 | 1.086 | 0.29 | 0.207 |
| | DBE 5 | 0.501 | 0.134 | 0.096 |
| | DBE 6 | 4.137 | 1.106 | 0.79 |
| | DBE 7 | 3.959 | 1.058 | 0.756 |
| Optimized Frame | DBE 1 | 0.007 | 0.001 | 0.001 |
| | DBE 2 | 0.018 | 0.002 | 0.002 |
| | DBE 3 | 0.012 | 0.002 | 0.001 |
| | DBE 4 | 0.009 | 0.001 | 0.001 |
| | DBE 5 | 0.004 | 0.0004997 | 0.000357 |
| | DBE 6 | 0.0001751 | 7.01E-05 | 3.50E-05 |
| | DBE 7 | 0.0001829 | 7.32E-05 | 3.66E-05 |

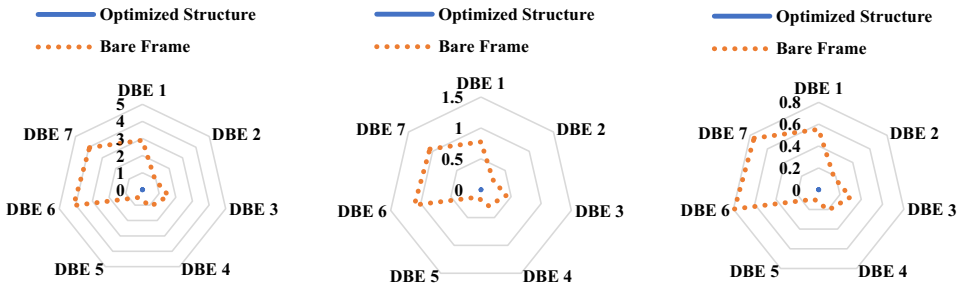


**(a)** Immediate occupancy **(b)** Life Safety **(c)** Collapse prevention

**Fig. 20** Demand-to-capacity ratio in the columns of the structure for DBE

**Table 16** Demand-to-capacity ratio of the columns in the bare frame for MCE

| Structure | Earthquake | Immediate occupancy | Life safety | Collapse prevention |
|---|---|---|---|---|
| Bare Frame | MCE 1 | 4.811 | 1.286 | 0.919 |
| | MCE 2 | 6.287 | 1.681 | 1.2 |
| | MCE 3 | 6.383 | 1.706 | 1.219 |
| | MCE 4 | 5.191 | 1.388 | 0.991 |
| | MCE 5 | 22.586 | 6.038 | 4.313 |
| | MCE 6 | 4.665 | 1.247 | 0.891 |
| | MCE 7 | 3.959 | 1.058 | 0.756 |
| Optimized Frame | MCE 1 | 0.062 | 0.009 | 0.006 |
| | MCE 2 | 0.096 | 0.017 | 0.009 |
| | MCE 3 | 0.01397486 | 0.0185471 | 0.013248 |
| | MCE 4 | 0.13 | 0.032 | 0.016 |
| | MCE 5 | 0.091 | 0.012 | 0.009 |
| | MCE 6 | 0.07164748 | 0.0950886 | 0.067921 |
| | MCE 7 | 0.064 | 0.013 | 0.007 |

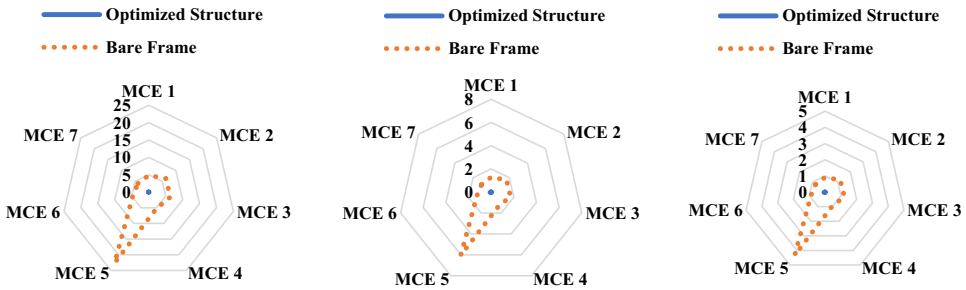


**(a)** Immediate occupancy **(b)** Life Safety **(c)** Collapse prevention

**Fig. 21** Demand-to-capacity ratio for MCE

## 9 Conclusions

The current research study developed a hybrid PSOGSA technique for the multi-objective optimization of a structure subjected to seismic excitations through the utilization of vibrational damper devices according to the performance-based design method. In this method, the details of the structural design, including the member sections and steel reinforcement, as well as the type and characteristics of the structural vibration damping system were optimized simultaneously to minimize the cost of construction and to satisfy the acceptance criteria for the performance-based design method, including structural movements and the occurrence of plastic hinges in the beams and columns.

For this purpose, seven types of structural damping systems were considered, and seven earthquake records

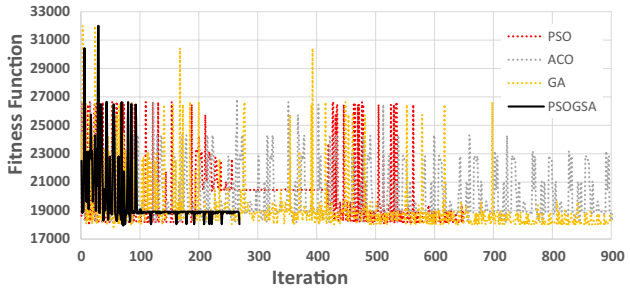


**Fig. 22** Comparison of the objective function during the optimization process

at the DBE and MCE levels were adopted for application to the structure.

The results proved that the developed PSOGSA optimization method was able to effectively minimize the effect of earthquakes on the structure through the utilization of an optimum design and vibration damping system. This technique also greatly improved the integrity and protection of the building against the applied DBE and MCE, as demonstrated by some of the highlighted results as follows:

- The outcome of this study proved that the reduction in the occurrence of plastic hinges in the optimized structure equipped with optimum damping devices was 100% for both the MCE and DBE levels. Therefore, it could be

**Fig. 23** Comparison of the percentage of the occurrence of plastic hinges during the optimization process

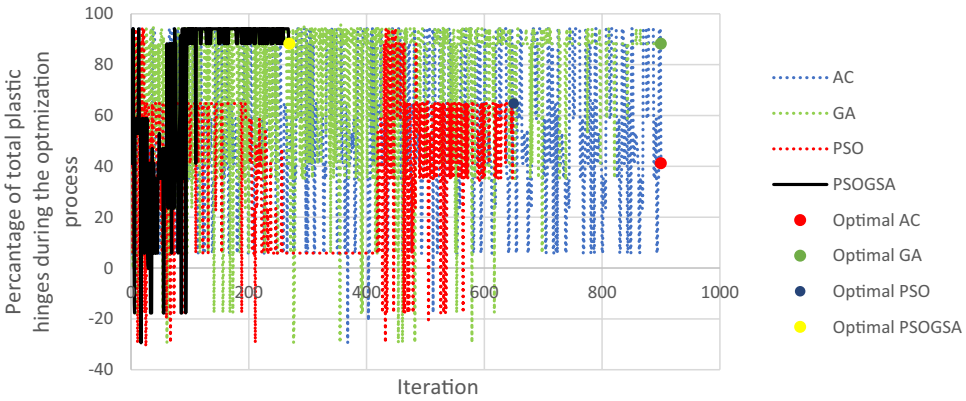


(a) DBE Level

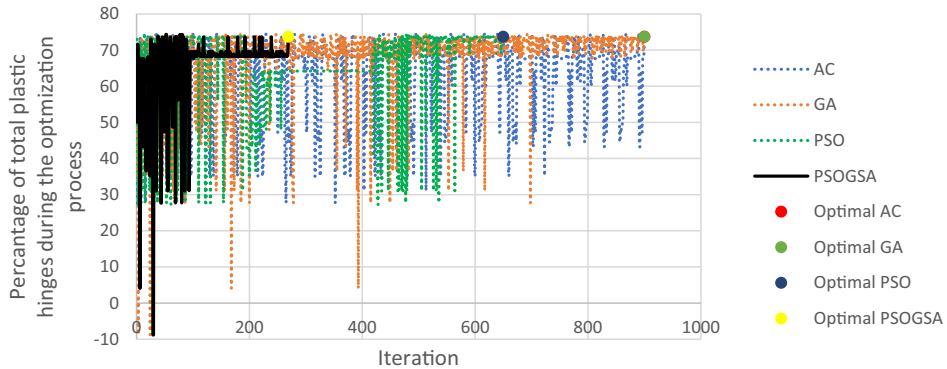


(b) MCE Level

**Table 17** Percentage of reduction in maximum and minimum displacements

| Optimization Method | Maximum displacement in the X-direction | | Minimum displacement in the X-direction | | Maximum displacement in the Y-direction | | Minimum displacement in the Y-direction | |
|---|---|---|---|---|---|---|---|---|
| | DBE level | MCE level | DBE level | MCE level | DBE level | MCE level | DBE level | MCE level |
| PSOGSA | 41% | 41% | 44% | 43% | 23% | 24% | %,27 | 26.5% |
| ACO | 43% | 43% | 38.4% | 38% | 27.4% | 27% | 24.1%, | 27.3% |
| GA | 41% | 41% | 44% | 36% | 23% | 24% | 24% | 26.5% |
| PSO | 43.7% | 43.7% | 38.7% | 38.6% | 28.2% | 26.6% | 26.7% | 28.2% |

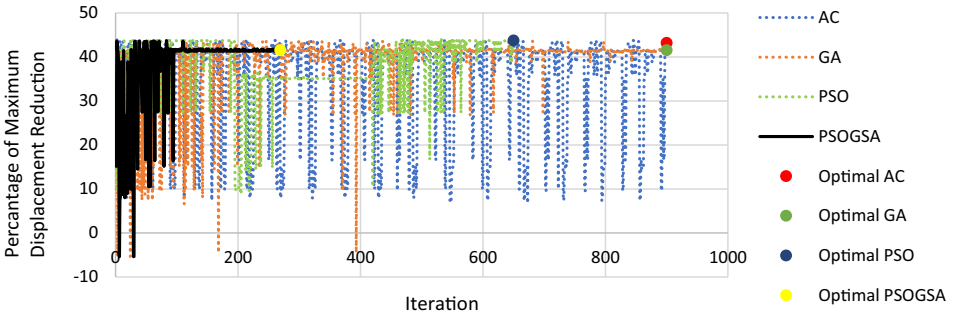


(a) Reduction in maximum positive displacement in X-direction

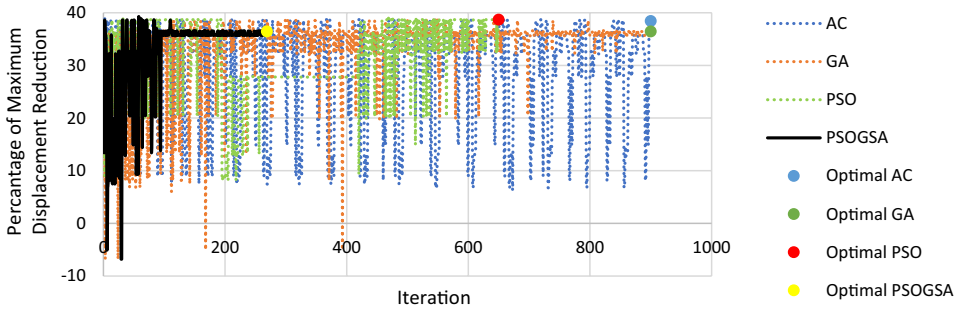


(b) Reduction in maximum negative displacement in X-direction

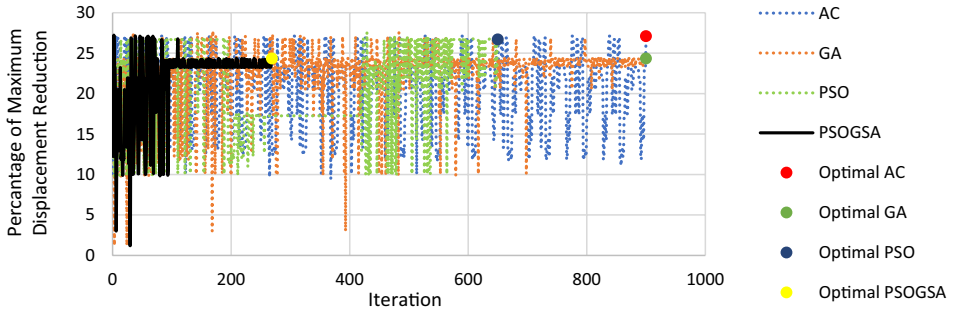


(c) Reduction in maximum positive displacement in Y-direction

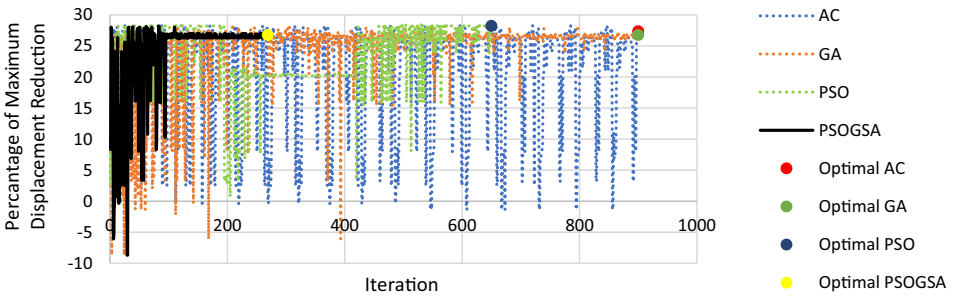


(d) Reduction in maximum negative displacement in Y-direction

**Fig. 24** Comparison of the reduction in the maximum displacement in the horizontal *X* and *Y*-directions during the optimization process for the DBE

concluded that the developed hybrid PSOGSA method effectively resulted in the optimum design of a structure equipped with the best vibration damping system that prevented any damage to the structural members, and thus, it was a more resilient structure compared to the bare frame.

- The results also indicated that the weight of the optimized structure was reduced by about 42% by minimizing the sectional area of the beams and columns, and the number and diameter of the steel bars, while also by considering the minimization of the displacement of the structure under applied seismic loads in the objective function.
- The displacement response of the optimized structure was reduced by about 41% and 23% in the *X*- and *Y*-directions under the applied MCE and DBE in comparison with the bare frame, which indicated the effec-

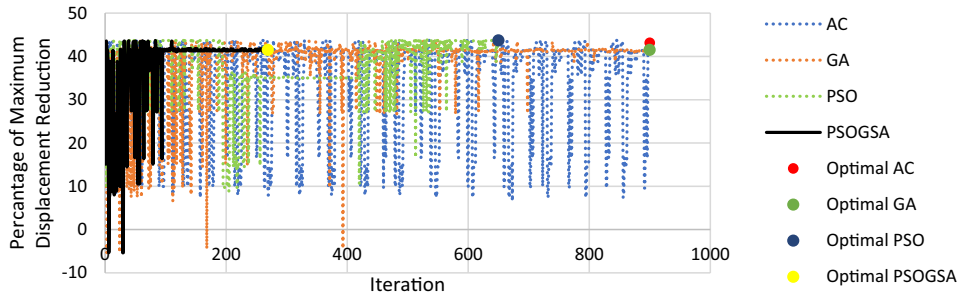


(a) Reduction in maximum positive displacement in X-direction

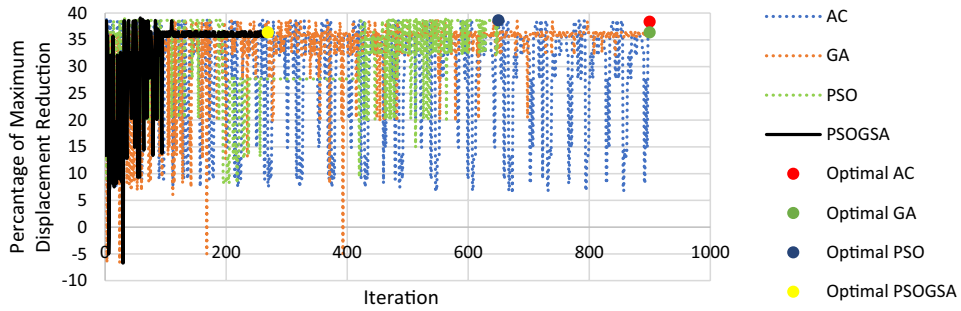


(b) Reduction in maximum negative displacement in X-direction

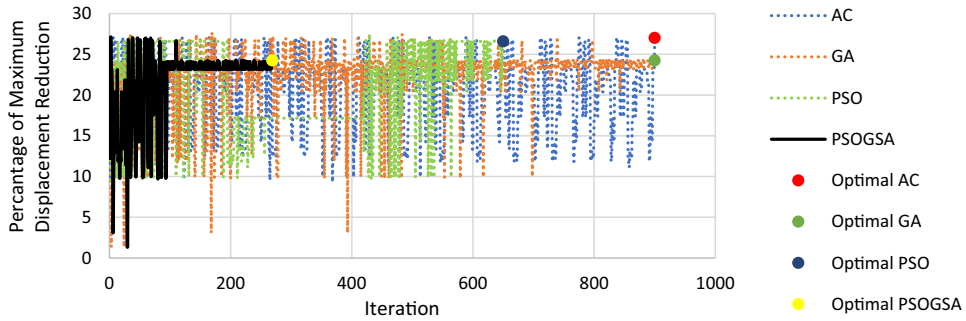


(c) Reduction in maximum positive displacement in Y-direction

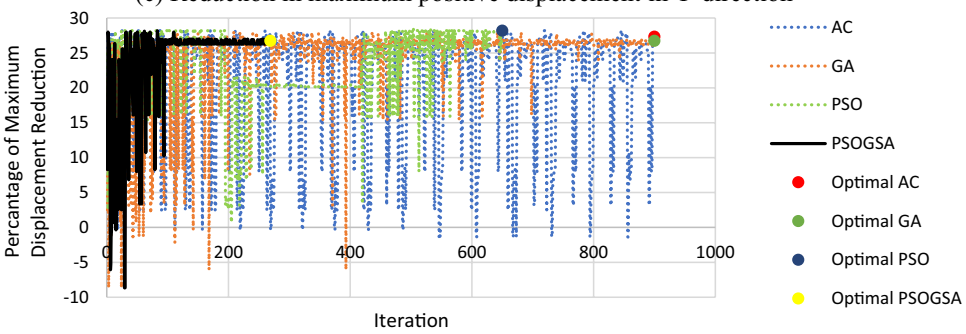


(d) Reduction in maximum negative displacement in Y-direction

**Fig. 25** Comparison of the reduction in the maximum displacement in the horizontal *X* and *Y*-directions during the optimization process for the MCE

tiveness of implementing the optimum damper devices to minimize movement of the structure.

- The inter-storey drift in the optimized design structure with the vibration dissipation system was reduced in the range of 34% to 47% for both the DBE and MCE records in comparison to the drifts in the bare frame.
- There was no formation of plastic hinges in the beam and column sections of the optimized structure, and it was revealed that the implementation of the optimum damper devices in the structure successfully diminished the effect of the DBE and even the MCE on the structure.
- The application of the optimum damping devices in the optimized structure resulted in a reduction in the base shear of the building in the range of 4% to 48% for the various applied DBE and MCE levels.

- A comparison of the PSOGSA technique with other optimization methods such as the genetic algorithm (GA), ant colony optimization (ACO), and particle swarm optimization (PSO) proved the high efficiency of this method in obtaining the optimum results with minimum computation time and effort. Therefore, the PSOGSA method exhibited a fast convergency rate in the range of 61% ~ 70% in comparison to the other optimization techniques that were studied.

**Data availability** All related data for this research are presented and available in the manuscript.

## Declarations

**Conflicts of interest** It is declared that there is no conflict of interest in this research work.

**Ethical standards** There are no ethical concerns in this research work.



## References

1. Rahimi F, Aghayari R, Samali B. Application of tuned mass dampers for structural vibration control: a state-of-the-art review. Civ Eng J. 2020;2:1622–51.
2. Ayyash N, Hejazi F. Development of hybrid optimization algorithm for structures furnished with seismic damper devices using the particle swarm optimization method and gravitational search algorithm. Earthq Eng Eng Vib. 2022;21(2):455–74.
3. Hejazi F, Farahpour H, Ayyash N, Chong T. Development of a volumetric compression restrainer for structures subjected to vibration. J Build Eng. 2022;46: 103735.
4. Malliotakis G, Alevras P, Baniotopoulos C. Recent advances in vibration control methods for wind turbine towers. Energies. 2021;14(22):7536.
5. Zareie S, Issa AS, Seethaler RJ, Zabihollah A. Recent advances in the applications of shape memory alloys in civil infrastructures: a review. In: structures. Amsterdam: Elsevier; 2020. p. 1535–50.
6. Cha Y-J, Agrawal AK, Phillips BM, Spencer BF. Direct performance-based design with 200kN MR dampers using multiobjective cost effective optimization for steel MRFs. Eng Struct. 2014;71:60–72.
7. Cha Y-J, Bai J-W. Seismic fragility estimates of a moment-resisting frame building controlled by MR dampers using performance-based design. Eng Struct. 2016;116:192–202.
8. García VJ, Duque EP, Inaudi JA, Márquez CO, Mera JD, Rios AC. Pendulum tuned mass damper: optimization and performance assessment in structures with elastoplastic behavior. Heliyon. 2021;7(6): e07221.
9. Xian J, Su C. Stochastic optimization of uncertain viscous dampers for energy-dissipation structures under random seismic excitations. *Mechanical Systems and Signal Processing*, *164*, 108208.20. *Minimum design loads for buildings and other structures.* Minimum Design Loads for Buildings and Other Structures, 1998, 2022.
10. Moghaddam H, Hajirasouliha I. Toward more rational criteria for determination of design earthquake forces. Int J Solids Struct. 2006;43(9):2631–45.
11. Moghaddam H, Hajirasouliha I. Optimum strength distribution for seismic design of tall buildings. Struct Des Tall Spec Build. 2008;17(2):331–49.
12. Hajirasouliha I, Doostan A. A simplified model for seismic response prediction of concentrically braced frames. Adv Eng Softw. 2010;41(3):497–505.
13. Hajirasouliha I, Pilakoutas K. General seismic load distribution for optimum performance-based design of shear-buildings. J Earthq Eng. 2012;16(4):443–62.
14. Nabid N, Hajirasouliha I, Petkovski M. Performance-based optimisation of RC frames with friction wall dampers using a low-cost optimisation method. Bull Earthq Eng. 2018;16(10):5017–40.
15. NEHRP Guidelines for the Seismic Rehabilitation of Buildings (FEMA 273), and NEHRP Commentary on the Guidelines for the Seismic Rehabilitation of Buildings (FEMA 274), (ATC 33), 1997.
16. Sahoo DR, Chao S-H. Performance-based plastic design method for buckling-restrained braced frames. Eng Struct. 2010;32(9):2950–8.
17. Gaxiola-Camacho JR, Azizsoltani H, Villegas-Mercado FJ, Haldar A. A novel reliability technique for implementation of performance-based seismic design of structures. Eng Struct. 2017;142:137–47.
18. Giannakouras P, Zeris C. Seismic performance of irregular RC frames designed according to the DDBD approach. Eng Struct. 2019;182:427–45.
19. Zhang C, Tian Y. Simplified performance-based optimal seismic design of reinforced concrete frame buildings. Eng Struct. 2019;185:15–25.
20. Asce. Seismic evaluation of existing buildings, 2003.
21. ACI 318-14. Building code requirements for structural concrete and commentary, 2014.
22. Mirjalili S, Hashim SZM. A new hybrid PSOGSA algorithm for function optimization. In 2010 International Conference on Computer and Information Application 2010
23. Kennedy J, Eberhart R. Particle swarm optimization. In: IEEE International Conference on Neural Networks–Conference Proceedings. 1995
24. Rashedi E, Nezamabadi-pour H, Saryazdi S. GSA: a gravitational search algorithm. Inf Sci. 2009;179(13):2232–48.
25. Adachi F, Yoshitomi S, Tsuji M, Takewaki I. Nonlinear optimal oil damper design in seismically controlled multi-story building frame. Soil Dyn Earthq Eng. 2013;44:1–13.
26. Hong SR, Wereley NM, Choi YT, Choi SB. Analytical and experimental validation of a nondimensional Bingham model for mixed-mode magnetorheological dampers. J Sound Vib. 2008;312(3):399–417.
27. Min K-W, Seong J-Y, Kim J. Simple design procedure of a friction damper for reducing seismic responses of a single-story structure. Eng Struct. 2010;32(11):3539–47.

28. Miyazaki M, Kitada Y, Arima F, Hristov I. 1986;1882–91
29. Rahman MM, Jadhav SM, Shahrooz BM. Seismic performance of reinforce concrete buildings designed according to codes in Bangladesh, India and US. Eng Struct. 2018;160:111–20.